Bone 57 (2013) 343–354

Contents lists available at ScienceDirect

Bone

journal homepage: www.elsevier.com/locate/bone

Original Full Length Article

After repeated division, bone marrow stromal cells express inhibitory factors with osteogenic capabilities, and EphA5 is a primary candidate ☆

Tsuyoshi Yamada [a,b], Masato Yuasa [a], Tomokazu Masaoka [a], Takashi Taniyama [a], Hidetsugu Maehara [a], Ichiro Torigoe [a], Toshitaka Yoshii [a], Kenichi Shinomiya [a], Atsushi Okawa [a,b], Shinichi Sotome [c,*]

[a] Department of Orthopaedic and Spinal Surgery, Graduate School, Tokyo Medical and Dental University, Tokyo, Japan
[b] Global Center of Excellence (GCOE) Program, International Research Center for Molecular Science in Tooth and Bone Diseases, Tokyo Medical and Dental University, Tokyo, Japan
[c] Section of Regenerative Therapeutics for Spine and Spinal Cord, Tokyo Medical and Dental University, Tokyo, Japan

ARTICLE INFO

Article history:
Received 1 May 2013
Revised 23 August 2013
Accepted 29 August 2013
Available online 9 September 2013

Edited by: R. Baron

Keywords:
Bone marrow stromal cells
Multi-lineage potential
Osteogenesis
Long-term culture
Cell–cell contact
EphA5

ABSTRACT

The differentiation capability of human bone marrow stromal cells (hBMSCs) is thought to deteriorate over multiple doubling processes. To clarify the deterioration mechanisms, the multilineage differentiation capabilities of short- and long-term passaged BMSCs were compared. Predictably, long-term passaged BMSCs showed reduced differentiation capacities compared to short-term passaged cells. Furthermore, a non-human primate heterotopic bone formation model demonstrated that long-term passaged BMSCs have bone formation capabilities but also exert inhibitory effects on bone formation. This finding indicated that long-term passaged BMSCs express higher levels of inhibitory factors than short-term passaged BMSCs do. Co-culture assays of short- and long-term passaged BMSCs suggested that the inhibitory signals required cell–cell contact and would therefore be expressed on the cell membrane. A microarray analysis of BMSCs identified ephrin type-A receptor 5 (EphA5) as an inhibitory factor candidate. Quantitative PCR revealed that among all members of the ephrin and Eph receptor families, only the expression of EphA5 was increased by BMSC proliferation. A gene knockdown analysis using siRNAs demonstrated that knockdown of EphA5 gene expression in long-term passaged BMSCs led to an increase in ALP mRNA expression. These results indicate that EphA5 may be a negative regulator of bone formation. A better understanding of the roles of the ephrin and Eph receptor families in hBMSCs may lead to alternative approaches for manipulating hBMSC fate. In addition, this avenue of discovery may provide new therapeutic targets and quality-control markers of the osteogenic differentiation capabilities of hBMSCs.

Introduction

Human bone marrow stromal cells (hBMSCs) are an attractive cell source for bone tissue engineering applications because they are available from adult bone marrow aspirates and have an excellent proliferation capability and a multipotent ability to differentiate into various types of mesenchymal lineages, such as osteogenic lineages [1,2].

For clinical tissue-engineered bone reconstructions, large amounts of hBMSCs are required and repeated cell multiplications are unavoidable. However, the differentiation potentials of these reconstructions deteriorate over multiple doubling processes and may not be sufficient for clinical applications once an adequate cell number is reached [3,4]. Moreover, the population of BMSCs is heterogeneous and contains subpopulations of osteoprogenitors and undifferentiated cells, and it is difficult to assess the overall profile of each batch of cells in a clinical setting [5]. There are two different reasons for the deterioration of the performance of BMSCs. The first is that the culture conditions may not adequately support the self-renewal of the stem cell within the BMSC population. The second is that as the cells expand, transiently amplifying cells (TACs) are generated and there is a dilution of the stem cell by these TACs, and their further differentiation into more committed cells. Deterioration may be the combination of both. Therefore, the deterioration of the quality of hBMSCs should be introduced to all clinicians for their use. The design of culture protocols to establish the optimum BMSCs that are able to retain their differentiation potential at an adequate level requires a more complete understanding of the deterioration mechanisms of these cells.

To increase the potential of the BMSCs to reconstruct damaged tissues, many studies have been conducted, but they primarily focused on growth factors, drugs, culture methods and scaffolding for tissue reconstruction. However, there are few reports that address the deterioration of BMSC potential by repeated doubling. Because our unpublished data

☆ Author contributions: T.Y.1: conception and design, experiments, data analysis and interpretation, and manuscript writing; M.Y.: experiments, surgery, and data analysis and interpretation; T.M., T.T., H.M., and I.T.: experiments, surgery, and data analysis; T.Y.2: experiments and data interpretation; A.O.: conception and design, data analysis and interpretation, and final approval of manuscript; S.S.: conception and design, experiments, surgery, data analysis and interpretation, and final approval of manuscript.

* Corresponding author at: Section of Regenerative Therapeutics for Spine and Spinal Cord, Tokyo Medical and Dental University, 1-5-45 Yushima, Bunkyo-ku, Tokyo 113-8519, Japan. Fax: +81 3 5803 5272.
E-mail address: sotome.orth@tmd.ac.jp (S. Sotome).

8756-3282/$ – see front matter © 2013 Elsevier Inc. All rights reserved.
http://dx.doi.org/10.1016/j.bone.2013.08.028

confirmed that a prolonged culture period of BMSCs impaired bone formation capability, we assumed that BMSCs expressed inhibitory factors for bone formation, and the expression levels of these factors increased with continued cell proliferation. In this study, we determined whether BMSCs expressed inhibitory factors against osteogenic differentiation and bone formation, which were measured by an in vivo bone formation study and in vitro assays. We also performed microarray analysis comparing BMSCs at a lower passage with BMSCs at a higher passage to determine whether there were any factors with increased expression after continued proliferation of the BMSCs. Among the factors identified, we focused on ephrin type-A receptor 5 (EphA5), a member of the ephrin receptor tyrosine kinase subfamily, as a candidate for the inhibitory factors. Recently, ephrins and the EphA receptors were reported to be involved in bone metabolism. Zhao et al. demonstrated that signaling between the extracellular domains of ephrinB2 expressed on osteoclasts and the ephrin type-B receptor 4 (EphB4) in osteoblasts suppresses osteoclast differentiation and stimulates osteogenic differentiation [6]. In addition to osteoclast–osteoblast interactions, osteoblast–osteoblast interactions through ephrinA2 and either ephrin type-A receptor 2 (EphA2) or EphA4 can also occur [7]. However, there have been no reports regarding EphA5 in bone metabolism.

The goals of the present study were to confirm the inhibitory effects of BMSCs and to identify the inhibitory factors involved in the deterioration of differentiation potential by comparing the gene expression profiles of long- and short-term cultured cells. The genes identified in this study may have the potential to act as new therapeutic targets and quality-control markers of the osteogenic differentiation capability of hBMSCs.

Materials and methods

Primary culture of hBMSCs

After obtaining informed consent, BMSCs were cultured from bone marrow aspirates of 34 patients who had received hip surgery at Tokyo Medical and Dental University under a protocol that was approved by the institutional review board. These donors ranged in age from 30 to 87 years old. Approximately 2 ml of bone marrow aspirate was obtained from the medullary cavity of the femoral shaft of each patient using a bone marrow biopsy needle (Cardinal Health, Dublin, OH, USA). The aspirate was added to 20 ml of standard medium (Dulbecco's modified Eagle's medium (DMEM), Sigma-Aldrich Co., St. Louis, MO, USA) containing 10% fetal bovine serum (Life Technologies Co., Carlsbad, CA, USA) and 1% antibiotic–antimycotic (10,000 U/ml penicillin G sodium, 10,000 μg/ml streptomycin sulfate and 25 μg/ml amphotericin B; Life Technologies) that contained 200 IU sodium heparin (Mochida Pharmaceutical Co. Ltd, Tokyo, Japan) and then centrifuged to remove the fat layer. Bone marrow cells were then resuspended in standard medium, and aliquots of the cell suspensions were used to count nucleated cell numbers after hemolysis. Subsequently, bone marrow cells, which included 1×10^8 nucleated cells, were plated into two 225-cm^2 flasks (Becton, Dickinson and Company, Franklin Lakes, NJ, USA). The cells were then cultured in each medium at 37 °C in a humidified atmosphere containing 95% air and 5% CO_2, and the medium was replaced every three days. When primary cultures became nearly confluent, the cells were detached with 0.25% trypsin containing 1 mM EDTA (Life Technologies) and subsequently replated for each assay. Cells were passaged at a density of 2×10^3 cells/cm^2, and hBMSCs at passages 1 (P1), P5, and P10 were stored in liquid nitrogen until further use. The collected hBMSCs were either cultured or preserved separately; the cells from individual donors were assayed independently to prevent cross contamination of hBMSCs from different donors.

Cell proliferation assay

BMSCs were plated at 5×10^3 cells/well in a 96-well culture plate. The cell number was counted at 1, 4, 7, and 10 days after seeding using the Cell Counting Kit-8 (Doujindo Molecular Technical Biology, Inc., Rockville, MD, USA) according to the manufacturer's instructions.

Osteogenic differentiation

BMSCs were replated at 2×10^3 cells/cm^2 in a six-well culture plate. When the culture plates became 80% confluent, the culture media of each group were changed to osteogenic media containing 10 mM β-glycerophosphate (β-GP, Sigma-Aldrich Co.) and 50 μg/ml ascorbic acid phosphate (AA, Wako, Osaka, Japan) [8] with or without 100 nM dexamethasone (DEX, Life Technologies) or BMP-2. After zero and seven days of osteogenic culture, the cells were used in each assay.

Chondrogenic differentiation

For chondrogenic induction, pellet culture was performed [9]. Briefly, after the culture medium was replaced with basal medium consisting of DMEM-high glucose with L-glutamine, sodium-pyruvate, pyridoxine hydrochloride (Life Technologies), 50 μg/ml ascorbic acid phosphate, 0.4 mM L-proline, 100 nM DEX, 1% ITS + 1 (Sigma-Aldrich Co.), and 10 ng/ml recombinant human TGF-β3 (Sigma-Aldrich Co.), 2.5×10^5 BMSCs were recentrifuged to obtain aggregated cells and cultured in 15-ml centrifuge tubes for 21 days.

Adipogenic differentiation

The BMSCs were replated at 2×10^3 cells/cm^2 and maintained until 80% confluency. Then, the culture medium was switched to adipogenic medium consisting of standard medium that was supplemented with 100 nM DEX, 500 μM isobutylmethylxanthine (Sigma-Aldrich Co.), and 100 μM indomethacin (Sigma-Aldrich Co.) for an additional 14 days.

RNA isolation and real-time PCR

Total ribonucleic acid (RNA) was isolated from the culture dishes using RNeasy Mini Kits (Qiagen, GmbH, Hilden, Germany), and first-strand complementary deoxyribonucleic acid (cDNA) was prepared using the PrimeScript RT reagent Kit with gDNA Eraser (Takara Bio Inc., Shiga, Japan) according to the manufacturer's instructions. Quantification of gene expression was analyzed by real-time polymerase chain reaction (PCR) using the Mx3000P® QPCR System (Agilent Technologies, Inc., Santa Clara, CA., USA) and the GoTaq® qPCR Master Mix (Promega Co., Fitchburg, WI, USA). Primer sets were predesigned and purchased from Takara Bio Inc. (Table 1). Standards were made from one specific sample, and every gene investigated in this study was run with a standard curve to quantify the relative Ct values of the samples. β-Actin was used to normalize the amount of template that was present in each sample.

ALP activity assay

Cells were washed with phosphate buffered solution (PBS), lysed with 500 μl of 0.2% Triton X-100 (Sigma-Aldrich Co.), and sonicated to destroy cell membranes. The supernatant (10 μl) was added to 100 μl of substrate buffer (10 mM disodium p-nitrophenylphosphate hexahydrate, 0.056 M 2-amino-2-methyl-1, 3-propanediol, and 1 mM $MgCl_2$; Wako) in a 96-well plate. After incubation at 37 °C for 30 min, the absorbance of each mixture at 405 nm was measured. The alkaline phosphatase (ALP) activity was determined using a standard curve and employed the reaction of 10 μl of a p-nitrophenyl solution (Wako) with 100 μl of substrate buffer for 30 min. The ALP activity was expressed as millimoles of p-nitrophenyl; to normalize the ALP activity, the DNA content was measured using the Quant-iT PicoGreen dsDNA Assay kit (Molecular Probes, Eugene, OR, USA) according to the manufacturer's instructions.

Table 1
RT-PCR primers used in this study.

Genes	Forward	Reverse
β-Act	TGGCACCCAGCACAATGAA	CTAAGTCATAGTCCGCCTAGAAGCA
ALP	GGACCATTCCCACGTCT	CCTTGTAGCCAGGCCCATTG
Runx2	CACTGGCGCTGCAACAAGA	CATTCCGGAGCTCAGCAGAATA
PPAR-γ	TGGAATTAGATGACAGCGACTTGG	CTGGAGCAGCTTGGCAAACA
LPL	CCAAACTGGTGGGACAGGATG	GCTCCAAGGCTGTATCCCAAGA
Ephrin-A1	TGATCGCCACACCGTCTTC	CAGCGTCTGCCACAGAGTGA
Ephrin-A2	CTGCCTGCGACTGAAGGTGTA	ACACGAGTTATTGCTGGTGAAGATG
Ephrin-A3	TCTGAGGATGAAGGTGTTCGTCTG	TTCTCAAGCTTGGGCACCTG
Ephrin-A4	TCGGCTTTGAGTTCTTACCTGGA	AGACACCTGGAGCCTCAAGCA
Ephrin-A5	TGCTGGCATGTCGGAGGTTA	ACTGCAAAGCAGGGCAGTACAAG
Ephrin-B1	CCAAGAACCTGGAGCCCGTA	AGATGATGTCCAGCTTGTCTCCAAT
Ephrin-B2	CTGCTGGATCAACCAGGAATAAAGA	TCCTGAAGCAATCCCTGCAAATA
Ephrin-B3	CTGTCTACTGGAACTCGGCGAATAA	CCGATCTGAGGGTACAGCACATAA
EphA1	CCTGTGCTGCAAGGTGTCTGA	GTGAAGATCCGATGGGCAATG
EphA2	GAGCTTTGGCATTGTCATGTGG	GCACTGCATCATGAGCTGGTAGA
EphA3	TTTGTCCTGGCAAGAACCTGAAC	TTCGGGCTCGGATTTGGA
EphA4	GCCGAGTGAGCTCCAATGCTA	GCCTGCATACACAAGGTGAAGCTA
EphA5	GCCCGGCAGTATGTGTCTGTAA	TCCATTGGGACGATCTGGTTC
EphA7	AGAACACTGTCCTCACACTTGACC	TGACAAGCATAAACCACCAGTTCTA
EphA8	CCTATGGAAGTCGGAAACATGGTC	AGAGCCCAGAAATTGGGTAAGAGTG
EphB1	GCCCAATGGCATCATCCTG	ATCAATCCTTGCTGTGTTGGTCTG
EphB2	GACCAAGAGCACACCTGTGATGA	CCACCAGCTGGATGACTGTGA
EphB3	AGACTCGGACTCTGCGGACA	GCTCACTCCACTCGAGGATCA
EphB4	ATGCCTGGAGTTACGGGATTG	TCCAGCATGAGCTGGTGGAG
EphB6	GACCAATGGGAACATCCTGGAC	CCCGCACCTGGAAACCATAG
ITGA5	TCTGCAGTTGCATTTCCGAGTC	GTAGGGCATCTTCAGGGCTTTGTA

Alizarin red S staining for matrix mineralization

After fourteen days of osteogenic culture, cells were fixed in 70% ethanol for 20 min at 4 °C and washed twice with PBS. The fixed cells were incubated for 1 h in a 4 mM Alizarin Red S (Sigma Aldrich Co.) solution (pH 4.1–4.3) at room temperature and then washed twice with water. Alizarin Red S staining was released from the cell matrix by incubation in cetyl-pyridinium chloride for 45 min, and the amount of released dye was quantified by measuring the absorbance at 520 nm. Absorbance was normalized to cell number counted in a hemocytometer.

Bone formation study

All animal experiments were conducted according to the guidelines of the Tokyo Medical and Dental University for the care and use of laboratory animals. To obtain monkey BMSCs (mBMSCs), bone marrow was aspirated from the femurs of *Macaca fascicularis* (male, five years old, 4–5 kg body weight, n = 4) under general anesthesia by intramuscular injection of medetomidine hydrochloride (0.1 mg/kg) and ketamine hydrochloride (10 mg/kg). mBMSCs were cultured in culture media. When primary cultures became nearly confluent, the cells were passaged at a density of 4×10^3 cells/cm^2, and P2 to P4 were subsequently passaged in the same manner. Cryopreserved P0 and P4 mBMSCs were stored in liquid nitrogen until further use. The cells were pre-cultured before implantation and then became P1 and P5, respectively. When the cultures became subconfluent, the culture medium was supplemented with the above-mentioned osteogenic reagents for four days, and the cultures were then used to prepare implants.

Preparation of the implants

Implants for the bone formation assay were prepared according to previous reports [10,11]. Briefly, to combine the cells and porous β-tricalcium phosphate (β-TCP) blocks (5 × 5 × 5 mm, porosity: 75%, pore size: 100–200 μm, Olympus Co., Tokyo, Japan) as scaffolds for bone formation, autologous blood plasma that contained citrate phosphate dextrose for anticoagulation at a ratio of 1:10 by volume was prepared. Detached mBMSCs (P1 and/or P5) were suspended in autologous plasma, and four groups of cell suspensions were prepared, as shown in Fig. 2B. The cell suspension (1 ml) was mixed with 150 μl of 2% calcium chloride and immediately introduced into porous β-TCP blocks under vacuum. When calcium chloride was added, fibrinogen that was present in the cell suspension began to transform to fibrin and form fibrin networks in the porous scaffolds within a few minutes. As a result, the P1 + P1 and P1 + P5 implants contained twice the number of the cells that were present in the P1 and P5 implants.

Transplantation

Under general anesthesia, the monkeys were placed in a prone position and shaved. The monkeys were then draped in the typical sterile manner, three incisions were made on each side of their backs, and three muscle pouches were created at each side. Three β-TCP blocks of each group were implanted into each pouch at random, and the implants were harvested for histological analysis five weeks after transplantation.

Histological analysis

The harvested composites were fixed in 10% neutral-buffered formalin and decalcified with K-CX solution (Falma, Tokyo, Japan). For each implant, 5 μm paraffin sections located 0.5, 1.5, 2.5, 3.5, and 4.5 mm from the surface were prepared. Each section was stained with hematoxylin and eosin, and bone-formation areas were measured using the Adobe Photoshop 7.0 software (San Jose, CA, USA).

Conditioned medium assay

Subconfluent hBMSC cultures (P2 and P6) were used to obtain conditioned medium. BMSC-conditioned media from eight donors were prepared from culture media that had been used for the hBMSC cultures for 72 h. After 72 h, the media were collected and centrifuged to remove cellular debris, and the supernatants were harvested and stored at −80 °C until further use. The control medium consisted of culture medium that had been incubated without BMSCs at 37 °C for 72 h. Human BMSCs at P3 from three different donors were plated at a density of 4×10^3 cells/cm^2 in standard medium and in triplicate samples per condition in six-well plates, and after obtaining a subconfluent layer, the cells were cultured in a total volume of 2.0 ml of pooled BMSC-conditioned medium or of control medium that had been supplemented with 10 mM β-glycerophosphate (Sigma-Aldrich Co.) and 50 μg/ml ascorbic acid phosphate (Wako, Osaka, Japan) for seven days or fourteen days. The cells were then evaluated by quantitative PCR and mineralization assays, respectively.

Co-culture experiments

BMSCs at P1 and P5 were plated onto 60 mm polystyrene dishes (Becton Dickinson and Company) that were divided into two compartments by a septum (KE-42-T, Shin-Etsu Chemical Co., Tokyo, Japan). The septum was made by using a syringe to inject silicone at the center line of a 60 mm culture dish 2–3 mm in height. After the silicone bond cured, the dish was sterilized by UV-irradiation, filled with culture medium and incubated for 24 h before use. Once cells were plated on one of the compartments, these cells could not migrate over the septum. These cells were seeded at 1.5×10^4 cells/cm^2, which was almost confluency, to avoid additional cell proliferation and populational alterations.

We divided the cells into the following four groups (as shown in Fig. 3C): P1 or P5 cells that were seeded into both compartments (P1 and P5 groups), P1 and P5 cells that were mixed homogeneously at a 1:1 ratio and seeded into both compartments (P1 + P5 group),

and P1 and P5 cells that were seeded into separate compartments to avoid cell–cell contact between those cells (P1/P5 group). The culture media were exchanged for each experiment on the day following the plating. A combination of the two compartments was harvested and ALP mRNA expression was measured after seven days.

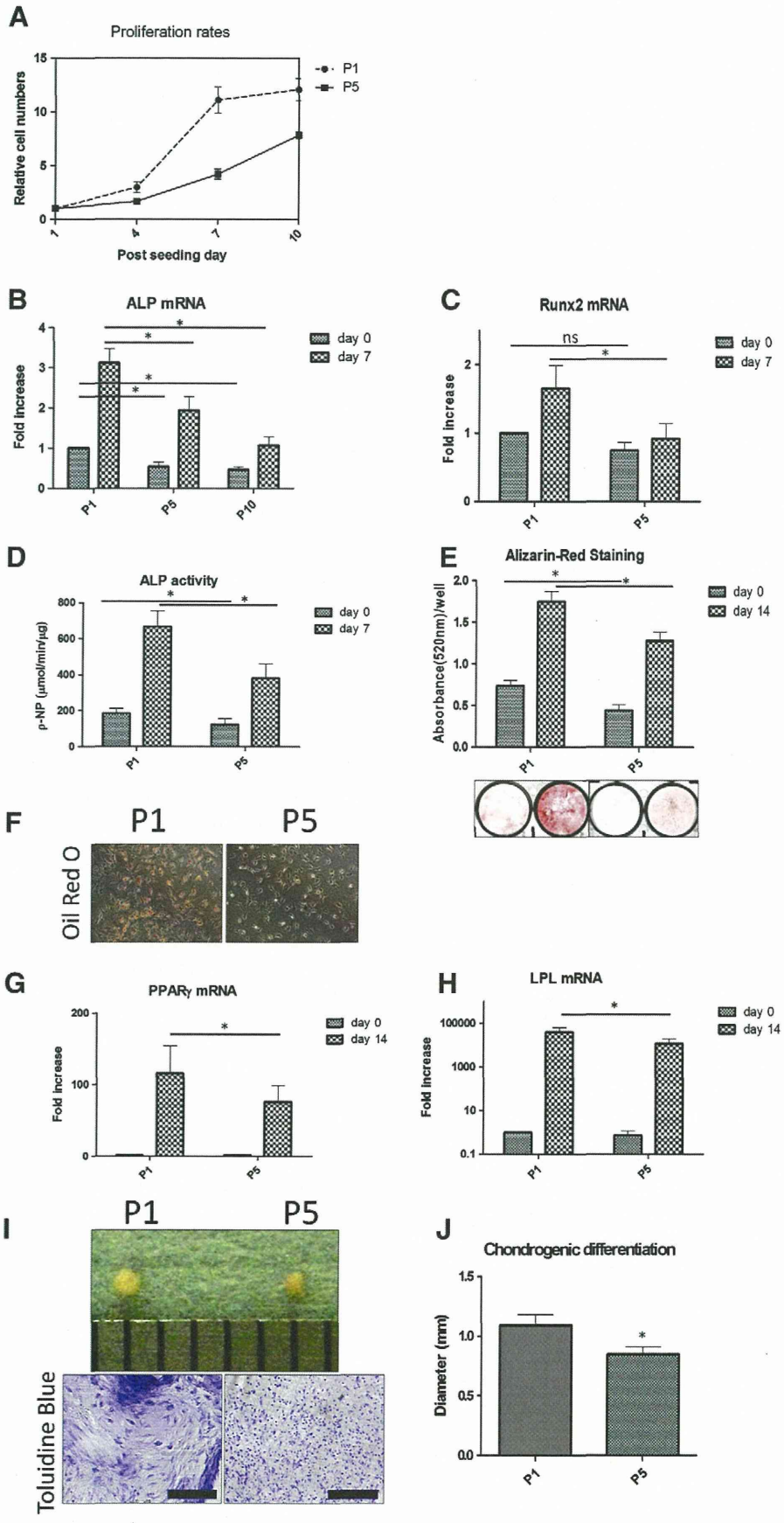

Microarray analysis

The total RNA from subconfluent BMSCs at P1 and P5 (day 0) was isolated and then treated with DNaseI for microarray analysis. One μg of total RNA was amplified and labeled with Cy3 or Cy5 using Ambion's Amino Allyl MessageAmp II aRNA Amplification Kit (Life Technologies, Cat #1753) according to the manufacturer's instructions. An Agilent Whole Human Genome Microarray 4 × 44 K (G4110F) was hybridized with 825 ng of amplified RNA at 65 °C for 16 h and washed using a fluidics station 450 (Affymetrix, Inc., Santa Clara, CA, USA). The microarray slides were scanned using a GenePix 4000B scanner from Axon Instruments (Union City, CA, USA), and each microarray image was first analyzed with the GenePix Pro 6.1 image analysis software (Molecular Devices, LLC, Sunnyvale, CA, USA) to derive the Cy3 and Cy5 fluorescent intensity and background noise for all of the spots on the array. The microarray data were normalized to the median, and $\log_2$ ratios were calculated versus the P1 groups of the corresponding donor sample. Genes that were more than threefold up- or down-regulated in the median of all donor samples were further classified according to their protein types through the SOSUI program.

Immunofluorescence staining

To minimize cell–cell contacts, the BMSCs were cultured at a low density (2×10^3 cells/cm^2) on 35 mm dishes and fixed in 4% paraformaldehyde (w/v) in PBS for 30 min. After washing in PBS, the BMSCs were incubated with 2% skim milk to eliminate non-specific binding. For the primary reaction, the BMSCs were incubated overnight with a 1:50 dilution of anti-EphA5 (Abcam, Cambridge, MA, USA, ab5397) antibody at 4 °C. After washing in PBS, the secondary antibody anti-rabbit Alexa Fluor 488 (Life Technologies) was applied to the cells at a dilution of 1:400 and incubated for 2 h at room temperature. In several experiments, the cells were also stained with 4′,6-diamidino-2-phenylindole (DAPI, 1:200) to visualize nuclei.

Western blot analysis

Proteins were extracted from the hBMSCs, the total cellular protein was prepared by lysing the cells in radioimmunoprecipitation assay (RIPA) buffer, and protein concentrations were determined using the BCA Protein Reagent Kit (Pierce, Rockford, IL, USA). Primary antibodies for EphA5 (AP7610d, Abgent, Inc., San Diego, CA., USA) and α-tublin (11H10; Rabbit mAb; #2125S, Cell Signaling Technology, Inc. Beverly, MA, USA) were obtained. Fifteen micrograms of protein was separated by 10% sodium dodecyl sulfate polyacrylamide gel electrophoresis (SDS-PAGE) and then transferred to a polyvinylidene difluoride (PVDF) membrane. After blocking with PVDF Blocking Reagent for Can Get Signal (Toyobo Life Science, Tokyo, Japan), the membranes were hybridized with primary antibody overnight at 4 °C and then hybridized with horseradish peroxidase (HRP)-linked anti-rabbit immunoglobulin G secondary antibody (#7074, Cell Signaling Technology, Inc., Tokyo, Japan) for 1 h at room temperature. Subsequently, Lumigen TMA-6 (Lumigen Inc., Southfield, MI, USA) was added onto the membrane and was allowed to stand for 2 min. The signals were detected by using an enhanced chemiluminescence method (ImageQuant LAS4000 Series; GE Healthcare UK Ltd, Buckinghamshire, England).

Gene knock-down studies

EphA5 gene silencing in BMSC cells at P5 by different DNA-modified siRNAs (ds RNA/DNA chimera: dsRDC) was performed. Seven small interfering RNAs (siRNAs) (dsRDCs) that were specific for human EphA5 were predicted using the Enhanced siDirect® program (RNAi Co., Tokyo, Japan) and synthesized by the Genosys siRNA service (Sigma Aldrich Co.). One of the siRNAs (siR-1) that targeted EphA5 was an oligoduplex of 5′CCAAAUUCGAGCAcgtacagc (sense) and 5′ tgtacgUG CUCGAAUUUGGAA (antisense). The other siRNA, siR-3, was composed of 5′ CACCAUUGAGAGAgttattgg (sense) and 5′ aataacUCUCUCAAU GGUGAU (antisense). The control siRNA, BannoNegaCon, was an oligoduplex of 5′GUACCGCACGUCAttcgtatc (sense) and 5′aataacU CUCUCAAUGGUGAU (anti-sense). For gene knock-down studies, the cells were seeded at 2000 cells/cm^2 in six-well plates and then cultured for 24 h. Cells at P5 were transfected with the siRNA (5 nM) with the aid of 10 μl of siRNA-MAX (Life Technologies). The overnight culture medium was replaced with osteogenic medium containing β-GP and AA, and the cells were further cultured for 72 h. Subsequently, total isolated RNA was quantitatively analyzed by real-time PCR.

Statistical analysis

The values were expressed as the arithmetic means ± standard error of the mean (S.E.M.) and analyzed using one-way analysis of variance (ANOVA). Then, Student's *t*-test was used for between-group comparisons. After the *p*-values were corrected using the Bonferroni correction, statistical significance was determined. Statistical significance is indicated by "*" in the graphs.

Results

Prolonged culture periods reduce the multi-lineage differentiation potential of BMSCs in vitro

We analyzed how the differentiation potential of BMSCs was affected by replicative senescence in vitro. Time course experiments showed that the hBMSCs at P1 grew more rapidly than the hBMSCs at P5 (Fig. 1A). The P1 cells took approximately 5–7 days to reach 80% confluence, whereas the P5 cells took 7–10 days. After accounting for the delay in differentiation due to the different proliferation rates and cell numbers, the culture medium of each group was changed to osteogenic medium when the culture plates showed a similar level of subconfluence.

At days 0 and 7 of osteogenic induction with DEX, total RNA of P1 and P5 cells was extracted from the culture, and quantification of gene expression was analyzed by real-time PCR. Whereas ALP and Runt-related transcription factor 2 (Runx2) mRNA expression at each passage were increased during osteogenic induction, the mRNA expressions of osteogenic markers at P5 were lower than those at P1 (Figs. 1B, C). Although individual differences were observed, the mRNA expression results of ALP were correlated with ALP activity and results from the mineralization assay (Figs. 1D, E). Owing to our previous data, in vitro ALP activity reflected bone formation capability of BMSCs [12], and the mRNA expression of ALP was used as a surrogate marker for osteogenic differentiation in subsequent experiments.

hBMSCs at different passages were simultaneously differentiated along adipogenic and chondrogenic lineages. Lipid accumulation was

Fig. 1. Multiple-lineage differentiation. Cell proliferation rates in P1 and P5 cultures. The fold change of cell counts was normalized to those of the P1 cell culture one day after plating (n = 4). The hBMSCs at P1 grow more rapidly than the hBMSCs at P5. (B–E) Osteogenic differentiation: Osteogenic supplements contained β-glycerophosphate, ascorbic acid phosphate, and DEX. (B, C) Quantitative analyses of mRNA expression of osteogenic markers: (B) ALP and (C) Runx2. The fold change of gene expression was normalized to that of the P1 cell culture at control day 0 (n = 12). (D) ALP activity (n = 12). (E) Alizarin red S staining. The absorbance of the extracted Alizarin red S stain was measured (n = 8). (F–H) Adipogenic differentiation. (F) Oil Red O (upper, Magnification × 40) (G) mRNA expression of PPARγ (H) and LPL at days 0 and 14 of adipogenic induction (n = 8). (I, J) Chondrogenic differentiation. (I) Chondrogenic pellets of the P1 and P5 groups after 21 days of chondrogenic culture (upper). Pellets were placed next to a 1 mm scale ruler. Toluidine blue staining of the pellets (lower). The scale bar indicates 100 μm. (J) The diameters of the pellets (n = 4).

visualized by Oil Red-O staining, and it was found that adipogenic induction was much more effective at P1 than at P5, which indicated that the adipogenic differentiation potential decreased in the course of in vitro proliferation. The expressions of peroxisome proliferator-activated receptor gamma (PPARγ) and lipoprotein lipase (LPL) mRNA at day 14 of adipogenic induction of P1 cells were significantly higher than that of P5 cells (Figs. 1F–H). For chondrogenic induction, pellet culture was performed, and it was found that the diameters of the pellets that were formed from P1 cells were significantly larger than those that were formed from P5 cells (Figs. 1I, J). These results support the notion that the multi-lineage differentiation potential of BMSCs deteriorated with increasing passages.

Long-term passaged hBMSCs exert inhibitory effects in vivo

We investigated how the extent of in vitro expansion of BMSCs affected the bone formation capability of BMSCs using a non-human primate heterotopic bone formation model. Histological analysis revealed that the implants that were prepared with P1 and P5 cells had bone formation capability; however, the P5 implants exhibited less bone formation than the P1 implants. Unexpectedly, despite an increased cell number, bone formation of the P1 + P5 implant decreased to half of that of the P1 implants in all four cases, whereas the P1 + P1 group exhibited increased bone formation compared to the P1 group (Figs. 2A, B). Based on these results, we presumed that the quality and not the quantity of the cells was important for effective bone regeneration and that long-term passaged P5 BMSCs exhibited bone formation capability and inhibitory effects on bone formation that were reinforced by proliferation of BMSCs.

Cell–cell contact inhibits the osteogenic differentiation potential in vitro

The identities of the inhibitory factors of bone formation are unknown. To investigate whether inhibitory signals were transmitted via cell–cell contact or by secreted factors, we prepared BMSC-conditioned medium using short- and long-term passaged cultures. If long-term passaged cells (P6) released the inhibitory factors as humoral factors, conditioned medium that was prepared from the cultures would contain the inhibitory factors. However, BMSCs in the conditioned medium from the P6 culture exhibited no deterioration in the mRNA expression of ALP or mineralization capability compared to the control or P2-conditioned medium (Figs. 3A, B). In contrast, some samples that were cultured in the conditioned medium showed higher expressions of ALP mRNA and mineralization capability than those cultured in fresh medium, which indicated that the hBMSC-conditioned medium might contain some up-regulators of differentiation capability.

To confirm that the inhibitory signals were transmitted via cell–cell contact, co-culture experiments were performed with or without cell–cell contact between P1 and P5 cells (Fig. 3C). The P1 BMSCs were completely separated from the P5 BMSCs, with only the culture medium shared between the P1 and P5 BMSCs. Because the cells were seeded to near confluence at the beginning of culturing to inhibit cell proliferation, the ratio of the P1 cells to the P5 cells in the P1 + P5 wells was almost identical to that in the P1/P5 wells. There was no significant difference between the P1 and P1 + P5 wells. In the P1 + P5 and P1/P5 culture, the medium from the P5 cells contained the secreted factors, but the medium of the P1 culture did not. Therefore, we believe that the difference between the culture media might affect the differentiation. Regardless of whether the osteogenic supplements were added or DEX or BMP was used during the osteogenic induction, the ALP mRNA

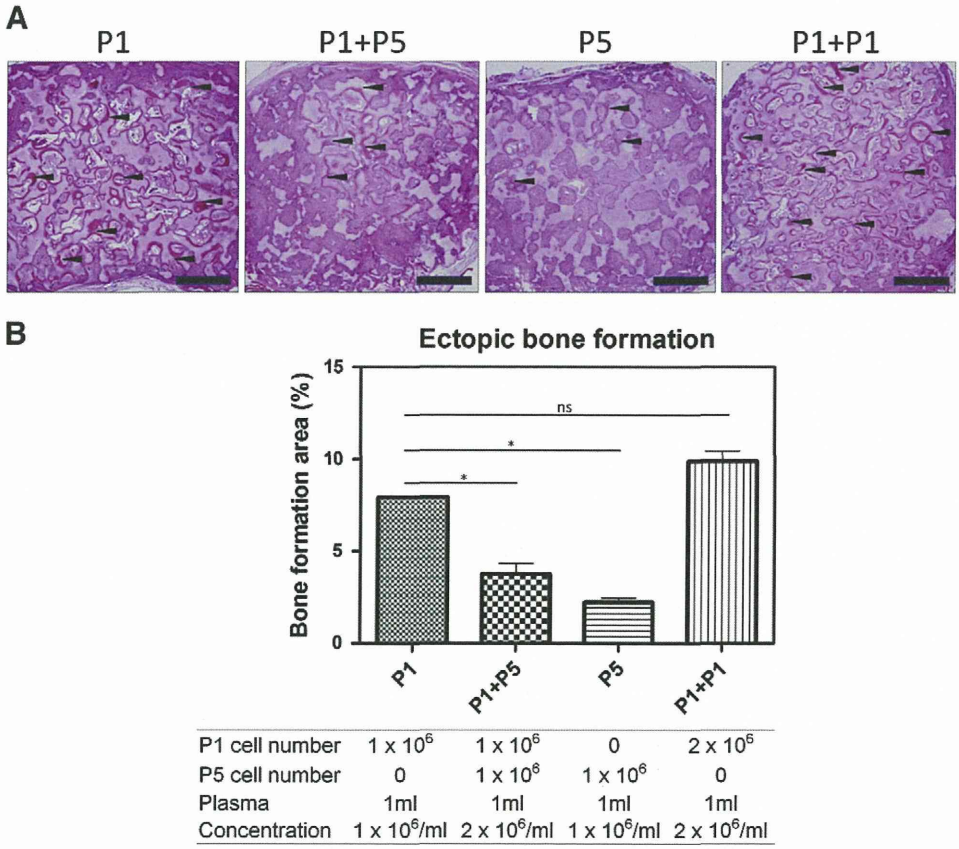

Fig. 2. Bone formation analyses. (A) In vivo bone formation analysis at extra-skeletal sites. Representative histological specimens at five weeks were stained with hematoxylin and eosin, and images were taken from the central portions of each implant. Scale bars indicate 1 mm, and arrowheads indicate newly formed bone. (B) Ectopic bone formation area (BFA) at five weeks. BFAs of the P1 group were significantly higher than those of the P5 group. BFAs of the P1 + P1 group at a double concentration of the P1 group (2×10^6 cells/ml) were higher, whereas those of the P1 + P5 group were significantly lower than those of the P1 group.

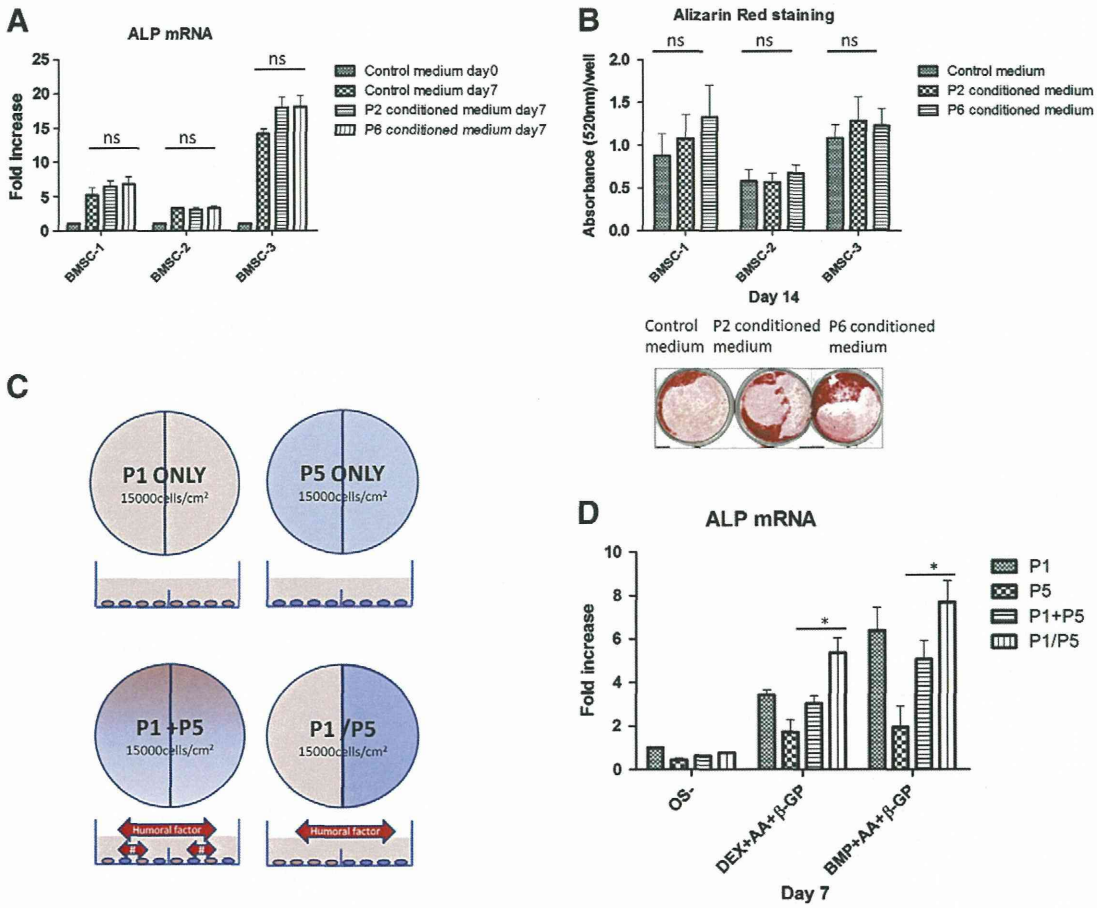

Fig. 3. BMSC-conditioned medium assays and co-culture assays. (A, B) BMSC-conditioned medium assays: (A) Quantitative analyses of mRNA expression of ALP. The fold change of gene expression was normalized to each cell culture in control medium at control day 0 (n = 4). (B) Alizarin red S staining and absorbance of the extracted Alizarin red S (n = 8). Three independent hBMSC preparations in conditioned media at P2 or P6. mRNA expression of ALP and the mineralization assay exhibited no deterioration compared to cells in control medium. (C, D) Co-culture assays. (C) Scheme of co-culture assays using the septum system on culture dishes. To investigate cell–cell contacts, cells at each passage were seeded at the indicated high-cell density and divided into four groups. In the P1 + P5 culture, intercellular contacts between the P1 and P5 cells occurred. In the P1/P5 culture, intercellular contact between the P1 and P5 cells was completely inhibited. # indicates intracellular contact between P1 and P5 cells. (D) Quantitative analyses of mRNA expression of ALP at day 7 of osteogenic induction. The fold change of gene expression was normalized to that of the P1 cell culture in standard medium at control day 7 ($n = 8$). The P1 + P5 group exhibited decreased expression of ALP mRNA compared to the separated P1/P5 group.

expression levels were reduced in the mixed P1 + P5 group compared to the separate P1/P5 group. In the latter group, cultured P1 and P5 cells were isolated from each other by a separator, in which the transportation of the culture medium and its contained factors was free (Fig. 3D). These data indicate that there may be factors that promote differentiation in the shared culture medium and that cell–cell contacts are involved in the deterioration of the differentiation capability of the cell.

Microarray analyses indicate an up-regulation of ephrin type-A receptor 5 (EphA5) genes in late culture

Microarray analysis was utilized to nominate candidate inhibitors that might be increased in P5 but not P1 cells (Table 2). Some genes that are associated with neuronal lineage, such as NTF3, leucine-rich repeat neuronal 3, and lipid phosphate phosphatase-related protein type 4, were up-regulated in the late stages of cell culture. Wnt signaling inhibitors, such as dickkopf 1 (DKK1), were also up-regulated, and secretion of these inhibitors in the later stages might suppress osteogenic differentiation. However, these factors were all secreted factors. Among the membrane proteins, EphA5, which is a receptor tyrosine kinase, showed the highest up-regulated ratio at P5, and the mRNA expression of this gene in all eight sample sets was up-regulated. Therefore, we focused on EphA5 as a candidate inhibitory factor of osteogenic differentiation.

EphA5 is up-regulated in late culture and down-regulated during osteogenic induction with DEX

To detect EphA5 in hBMSCs and the alternation of expression of EphA5 by repeating passages, immunofluorescence staining was performed. This analysis thoroughly detected EphA5 molecules in all P5 cells, and the detected fluorescence in P5 cells was more intense than that in P1 cells (Fig. 4A). Quantitative PCR and Western blot analyses demonstrated that EphA5 mRNA and proteins were more strongly detected in P5 than in P1 cells (Fig. 4B), respectively. EphA5 decreased with time in osteogenic culture (day7). This was with the addition of osteogenic supplements including DEX.

In previous studies, several molecules, such as ephrin-A5 and EphA2-5, were expressed on the surface of osteoblasts or preosteoblasts [7,13]. Using real-time PCR, we analyzed the expression of all known members of the ephrin and Eph families in the hBMSC cultures. Various subtypes of ephrins and Eph receptors were expressed in hBMSCs (Fig. 5A), and among these, only EphA5 expression was up-regulated at P5, whereas repeating passages suppressed the levels of ephrin-B1, B3, EphB2, EphB4, and EphB6 (Fig. 5B).

Our data revealed that various subtypes of at least four EphA receptors (EphA2, A3, A4, and A5), four EphB receptors (EphB1, B2, B3, and B4), and their ligands (ephrin-A3, A4, A5, B1, and B2) were expressed in hBMSCs, which resulted in a characteristic that resembled osteoblasts

Table 2
Human genes up- and down-regulated three-fold or higher in hBMSCs at P1 compared with those at P5.

Genes		GenBank	SOSUI	Log_2 ratio
SERPINB2	Serpin peptidase inhibitor, clade B (ovalbumin), member 2	NM_002575	Soluble protein	4.382
EPHA5	EPH receptor A5	NM_004439	Membrane protein	3.563
SCN9A	Sodium channel, voltage-gated, type IX, alpha	NM_002977	Membrane protein	3.393
NTF3	Neurotrophin 3	NM_002527	Secretory protein	2.654
SCIN	Scinderin	NM_033128	Soluble protein	2.462
RGS7	Regulator of G-protein signaling 7	NM_002924	Soluble protein	2.326
FOXQ1	Forkhead box Q1	NM_033260	Soluble protein	2.280
LRRN3	Leucine rich repeat neuronal 3	NM_018334	Secretory protein	2.263
PRSS3	Protease, serine, 3 (mesotrypsin)	NM_002771	Secretory protein	2.191
PTGIS	Prostaglandin I2 (prostacyclin) synthase	NM_000961	Secretory protein	2.132
SLC16A6	Solute carrier family 16, member 6 (monocarboxylic acid transporter 7)	NM_004694	Membrane protein	2.104
LRRN3	Leucine rich repeat neuronal 3 (LRRN3)	NM_018334	Secretory protein	2.004
DKK1	Dickkopf homolog 1 (*Xenopus laevis*)	NM_012242	Secretory protein	1.989
MYOZ2	Myozenin 2	NM_016599	Soluble protein	1.973
FLG	Filaggrin	NM_002016	Secretory protein	1.972
ANKRD29	Ankyrin repeat domain 29	NM_173505	Soluble protein	1.957
TSPAN8	Tetraspanin 8	NM_004616	Membrane protein	1.941
MEOX2	Mesenchyme homeobox 2	NM_005924	Soluble protein	1.902
PRSS2	Protease, serine, 2 (trypsin 2), transcript variant 1	NM_002770	Secretory protein	1.861
BMP6	Bone morphogenetic protein 6	NM_001718	Soluble protein	1.743
LPPR4	Plasticity related gene 1 (LPPR4)	NM_014839	Membrane protein	1.741
GATA6	GATA binding protein 6	NM_005257	Soluble protein	1.717
PPP1R14C	Protein phosphatase 1, regulatory (inhibitor) subunit 14C	NM_030949	Soluble protein	1.654
MFAP5	Microfibrillar associated protein 5	NM_003480	Secretory protein	1.643
MYPN	Myopalladin	NM_032578	Soluble protein	1.602
ACP5	Acid phosphatase 5, tartrate resistant	NM_001611	Secretory protein	−3.276
TYROBP	TYRO protein tyrosine kinase binding protein	NM_003332	Secretory protein	−2.809
IGLL1	Immunoglobulin lambda-like polypeptide 1, transcript variant 1	NM_020070	Soluble protein	−2.750
LCP1	Lymphocyte cytosolic protein 1 (L-plastin)	NM_002298	Soluble protein	−2.574
ACTG2	Actin, gamma 2, smooth muscle, enteric	NM_001615	Soluble protein	−2.391
RBP1	Retinol binding protein 1, cellular	NM_002899	Soluble protein	−2.383
IGJ	Immunoglobulin J polypeptide, linker protein for immunoglobulin alpha and mu polypeptides	NM_144646	Secretory protein	−2.319
NUDT10	Nudix (nucleoside diphosphate linked moiety X)-type motif 10	NM_153183	Soluble protein	−2.287
CES1	Carboxylesterase 1 (monocyte/macrophage serine esterase 1), transcript variant 3	NM_001266	Secretory protein	−2.078
PARP4	Poly(ADP-ribose) polymerase family, member 4	NM_006437	Secretory protein	−1.942
SMOC2	SPARC related modular calcium binding 2	NM_022138	Secretory protein	−1.892
ZNF626	Zinc finger protein 626, transcript variant 1	NM_001076675	Soluble protein	−1.892
CDCA7	Cell division cycle associated 7, transcript variant 1	NM_031942	Soluble protein	−1.880
RNASE1	Ribonuclease, RNase A family, 1 (pancreatic), transcript variant 3	NM_198232	Secretory protein	−1.855
SFRP1	Secreted frizzled-related protein 1	NM_003012	Secretory protein	−1.850
APOC1	Apolipoprotein C-I	NM_001645	Secretory protein	−1.759
IGFBP2	Insulin-like growth factor binding protein 2, 36 kDa	NM_000597	Secretory protein	−1.743
SOX11	SRY (sex determining region Y)-box 11	NM_003108	Soluble protein	−1.668

A total of 21,050 human genes consistent with the quality criteria, genes up- and down-regulated three-fold or higher are listed.

(Figs. 5A, B). As mentioned before, among the ephrin and Eph families, only EphA5 expression was up-regulated at P5, and this expression was suppressed by adding osteogenic supplements, such as DEX (AA + β-GP + DEX). Similarly, osteogenic induction using DEX suppressed the mRNA expression levels of ephrin-B1, EphA2, EphB1, EphB2, and EphB3, whereas it increased those of ephrin-B2 and EphB6. When BMP-2 was used as an osteogenic reagent (AA + β-GP + BMP-2), alteration patterns during osteogenic induction of some

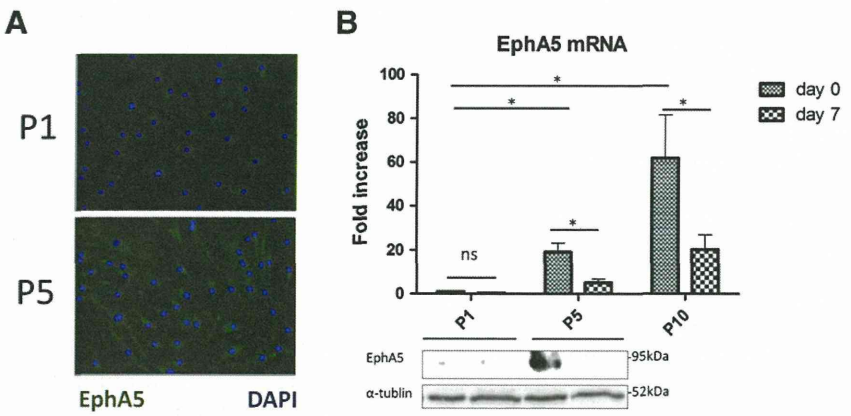

Fig. 4. Expression of EphA5. (A) Immunofluorescence staining of EphA5. Magnification × 100. (B) Quantitative analyses of mRNA expression of EphA5 (upper) and EphA5 protein (lower: Western blot). The fold change of gene expression was normalized to that of the P1 cell culture at control day 0 (n = 12).

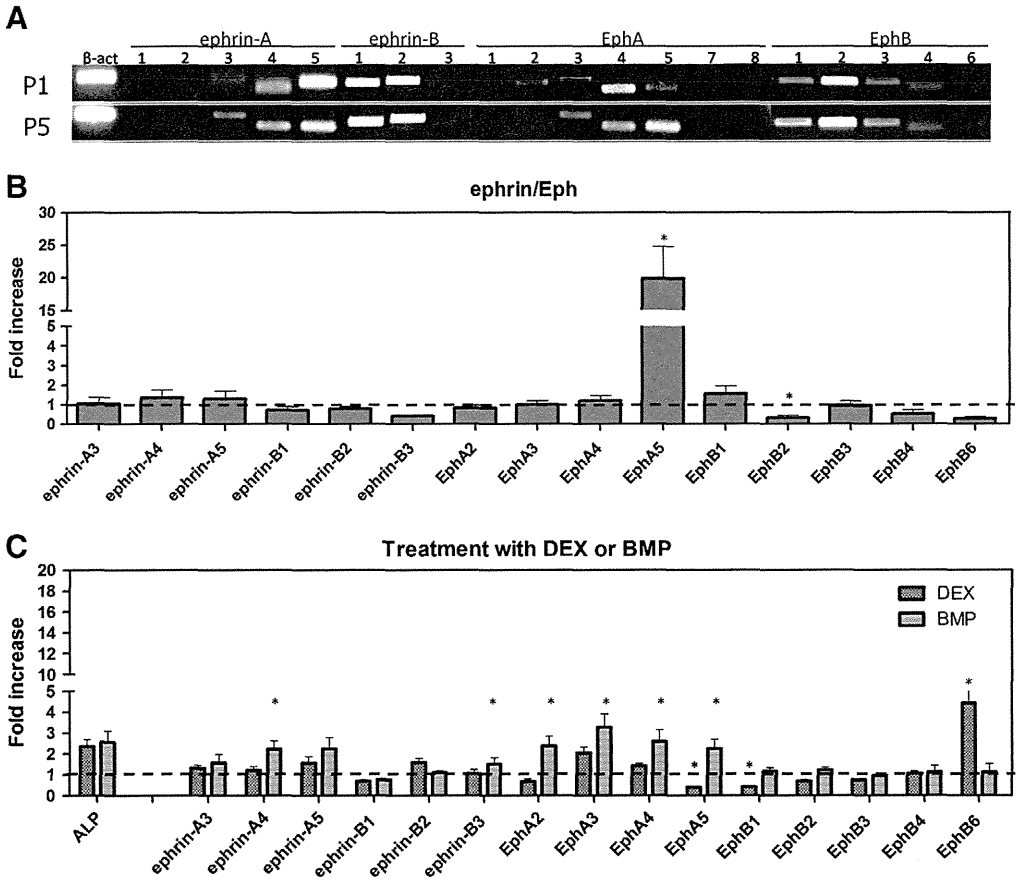

Fig. 5. Expression of members of the ephrin and Eph receptor families in hBMSCs. (A) Representative RT-PCR analysis of BMSCs from the P1 and P5 cultures. (B) Quantitative analyses of mRNA expression of members of the ephrin and Eph receptor families in hBMSCs of the P5 culture. Fold change of gene expression was normalized to the P1 cell culture. (C) BMSCs of the P5 culture were differentiated into osteogenic lineages using AA+β-GP+DEX or BMP-2, and quantitative PCR of ephrin and Eph receptor family mRNA expression were performed at day 3 of osteogenic induction (n = 8). Fold change of gene expression was normalized to the non-treatment culture.

ephrins and Eph receptors differed from those during osteogenic induction using DEX (Fig. 5C). DEX did reduce EphA5, but BMP-2 did not.

siRNA-mediated silencing of EphA5 promotes osteogenic differentiation in hBMSCs

To further establish the role of EphA5 in hBMSC osteoblast differentiation, we determined whether RNAi-mediated silencing of EphA5 expression promoted the expression of an osteogenic marker, ALP. Silencing of EphA5 expression using two different siRNAs decreased EphA5 mRNA by 80% after three days (Fig. 6A), whereas an irrelevant control siRNA had no effect. In contrast to the control siRNA, treatment with EphA5 siRNA led to increases in ALP and Runx2 levels (Figs. 6B, C), which indicated that EphA5 was required to suppress the osteoblast phenotype in hBMSCs. Down-regulation of EphA5 also resulted in up-regulated integrin alpha 5 (ITGA5) levels (Fig. 6D).

Discussion

BMCSs that have multi-lineage differentiation potential have been expected to be cell sources for tissue-engineered regenerative medicine of various organs. However, it is also well known that their differentiation potential deteriorated due to the multiple doubling processes required to obtain sufficient cell numbers for use [3,4,14,15]. In our in vitro differentiation assays using hBMSCs, we demonstrated that the osteogenic differentiation capability and adipogenic and chondrogenic differentiation capability of the cells decreased after multiple passages. The following two mechanisms and the combination of the two were assumed: the differentiation capability of each cell that composed BMSCs decreased due to senescence by repeated cell division, and compositional alteration of BMSCs during proliferation contained multiple subpopulations with various differentiation and proliferation capabilities. Our previous report demonstrated that BMSCs that were cultured with continuous DEX treatment exhibited different cell proliferation and altered subpopulations [16]; therefore, BMSCs with continuous treatment were more capable of differentiating into multiple lineages. In this report, BMSCs that were continuously treated with DEX expressed much higher ALP levels, which is a marker of both osteogenic lineage and the undifferentiated stage of stem cells. Therefore, we supposed that ALP was an osteogenic marker and a marker in pluripotency. We can use ALP activity and mRNA expressions to judge which BMSCs are preferred for use in bone tissue engineering [12].

Using a non-human primate ectopic bone formation model, we demonstrated that adding long-term cultured BMSCs to short-term cultured BMSCs decreased bone formation areas by 50% compared to that of short-term cultured BMSCs alone, and this decrease occurred even if the long-term cultured BMSCs had osteogenic capability that was sufficient for bone formation in vivo. This assay revealed that long-term passaged BMSCs had bone formation capability but could also inhibit bone formation. While many reports have focused on osteogenic stimulators that are expressed in BMSCs, such as growth factors and chemokines [7–13], few studies have investigated inhibitors that decrease bone formation by BMSCs and are expressed in BMSCs. An BMSC-conditioned medium assay showed relatively higher expressions

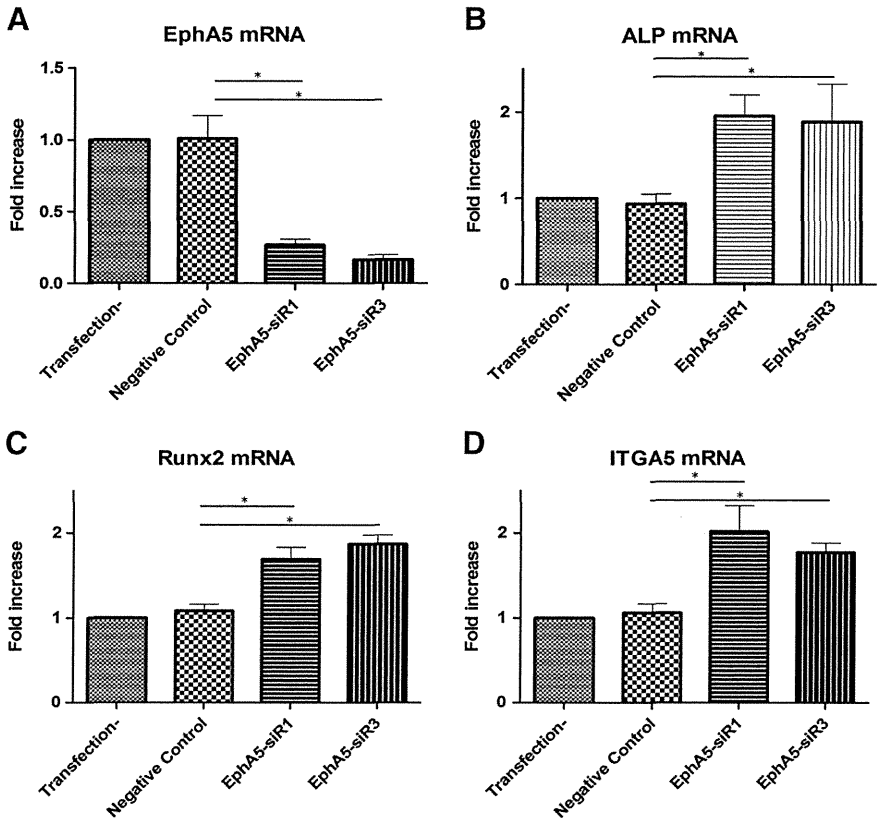

Fig. 6. EphA5 gene silencing in hBMSCs by siRNAs. EphA5 gene silencing in hBMSCs by two different siRNAs, siR-1 and siR3. hBMSCs were transfected with the respective siRNA or control siRNA, and mRNA expression of EphA5 (A), ALP (B), Runx2 (C) and ITGA5 (D) was quantified three days after transfection ($n = 7$). The fold change of gene expression was normalized to the untreated culture.

of ALP mRNA and mineralization in some samples than those cultured in the standard medium, which indicated that the BMSC-conditioned medium might contain both growth factors/chemokines and inhibitors that in toto, lead to up-regulate their differentiation capability. Consistently, Osugi et al. reported the use of stem-cell-cultured conditioned media that utilized paracrine factors of stem cells for bone regeneration [17]. Furthermore, co-culture assays provided evidence for the existence of hBMSC osteogenic inhibitors whose function was mediated by cell–cell contact.

To identify osteogenic inhibitors, we compared the expression of mRNAs in P1 and P5 BMSCs using microarray analysis. Based on the obtained results, we hypothesized that some factors that decreased the differentiation capability of BMSCs via cell–cell contact were expressed in BMSCs and that this expression increased during the proliferation process. The expression of many genes was up-regulated in BMSCs at P5, but EphA5 was the only gene that was up-regulated in all eight sample sets and was expressed on the cell membrane. However, a previous report by Irie et al. showed that EphA5 was not detected in differentiating calvarial osteoblasts from C57BL/6J mice until 10 days of differentiation in culture [7]. In our study, EphA5 was barely detected in the hBMSCs at early passages but showed increased expression levels in later passages. Increased expression of EphA5 in late stage hBMSCs was also reported by Tanabe et al. [5], though the effects of EphA5 on osteogenic differentiation were not analyzed; thus, no information regarding the effects of EphA5 on osteogenesis and bone metabolism was available.

EphA5 is a member of the ephrin receptor tyrosine kinase subfamily and can bind ephrin-A1, A2, A3, A4, and A5. The ephrin receptors are divided into two groups based on the similarity of their extracellular domain sequences and their affinities for binding ephrin-A and ephrin-B ligands, and they constitute the largest subfamily of receptor protein tyrosine kinases. These receptors have the ability to induce forward and reverse (bi-directional) signaling between adjacent interacting cells [18–21], and increasing evidence has suggested that the Eph receptors are capable of unconventional signaling activities that do not depend on activation by ephrin ligands [22,23].

Eph and Eph-related receptors have been implicated in mediating developmental events, particularly in the nervous system [24–30]. The roles of the Eph receptors and ephrin ligands in cell adhesion, migration [31–33], formation of the borders of compartments [34–36], regulation of cell proliferation in various tumors [37–43], angiogenesis [44,45], immunity [46], and regulation of insulin secretion [47,48] are also well documented; however, their potential role in bone biology is only now beginning to emerge. Several recent studies have suggested that certain axon-guidance molecules are involved in the cell–cell communication between osteoclasts and osteoblasts [49,50], and the functions of ephrin-B2 in osteoclasts and EphB4 in osteoblasts were found to be associated with the switch from bone resorption to bone formation [6,51]. Furthermore, bidirectional signaling through ephrin-A2–EphA2 enhanced osteoclastogenesis and suppressed osteoblastogenesis at the initiation phase of bone remodeling [7], and EphA4 in osteoblasts executed the final process of endochondral bone formation [52]. Additionally, regulation of integrin activities has been demonstrated to be a key mechanism that underpins the effects of ephrin and the Eph system on cell–matrix adhesion and migration. For example, ephrin-A signaling activates the integrin pathway, thereby increasing cell adhesion or changing the morphology and motility of cells [46,53,54]. EphA–ephrin-A binding also induces integrin clustering for cell segregation during development [55]. In this study, downregulation of EphA5 induced by siRNA affected ITGA5 levels (Fig. 6C). Therefore, EphA5 down-regulation that is induced by DEX might activate ITGA5 [56], resulting in an increased osteoblast differentiation and osteogenesis in vitro.

Whereas the expression of some ephrin and Eph receptors was altered to some extent during proliferation, EphA5 expression at P5 exhibited a prominent increase compared to that at P1. Each class of ephrin does not necessarily bind to a single class of Eph receptor, and each Eph receptor does not necessarily bind to a specific class of ephrin. Therefore, the prominent expression of EphA5 could affect the signals that were transmitted between other Eph receptors and ephrins by competitive inhibition and could thus affect bone formation because ephrin-Eph receptor signals are involved in bone formation, as mentioned above. If EphA5 is not expressed until the cells undergo repetitive proliferation, this gene might exert minimal influence on bone metabolism under normal conditions, and the effects of EphA5 expression might be a specific issue when BMSCs are used in bone regeneration.

Down-regulation of endogenous EphA5 levels using siRNAs promoted osteogenic differentiation at day 3 of the study. The differences between the experimental and control groups decreased seven days after the initiation of knockdown (data not shown). We also attempted stable knockdown using lentiviral vectors with shRNA. However, the transfection efficiencies were low; thus, stable EphA5 knockdown in BMSCs was not achieved. We believe this limitation of this study could be addressed in future experiments. Although off-target effects of the siRNAs on genes other than EphA5 could not be completely excluded, the results of up-regulation of ALP expression three days into the knockdown study reinforced the possibility that EphA5 is a negative regulator of bone formation.

Conclusion

The multiple differentiation potential of hBMSCs deteriorated after the repeated passages that were required to obtain adequate cell numbers for clinical use. Inhibitory factors that transmitted signals via cell–cell contacts and were expressed in BMSCs were identified to take part in the mechanism of this deterioration. The expression of EphA5 was prominently up-regulated by proliferation, and this molecule was a convincing candidate for the inhibitory factor.

Disclosure of potential conflicts of interest

The authors declare that they have no competing interests.

Acknowledgments

We gratefully thank Dr. Tetsuya Jinno and Dr. Daisuke Koga for the collection of bone marrow aspirates during the operation procedure. This work was supported by a Grant-in-Aid for Scientific Research from the Japan Society for the Promotion of Science and from the General Insurance Association of Japan. We also acknowledge Olympus Co. for kindly donating the β-TCP ceramic blocks.

References

[1] Pittenger MF, Mackay AM, Beck SC, Jaiswal RK, Douglas R, Mosca JD, et al. Multilineage potential of adult human mesenchymal stem cells. Science 1999;284:143–7.
[2] Prockop DJ. Marrow stromal cells as stem cells for nonhematopoietic tissues. Science 1997;276:71–4.
[3] Vacanti V, Kong E, Suzuki G, Sato K, Canty JM, Lee T. Phenotypic changes of adult porcine mesenchymal stem cells induced by prolonged passaging in culture. J Cell Physiol 2005;205:194–201.
[4] Wagner W, Horn P, Castoldi M, Diehlmann A, Bork S, Saffrich R, et al. Replicative senescence of mesenchymal stem cells: a continuous and organized process. PLoS One 2008;3:e2213.
[5] Tanabe S, Sato Y, Suzuki T, Nagao T, Yamaguchi T. Gene expression profiling of human mesenchymal stem cells for identification of novel markers in early- and late-stage cell culture. J Biochem 2008;144:399–408.
[6] Zhao C, Irie N, Takada Y, Shimoda K, Miyamoto T, Nishiwaki T, et al. Bidirectional ephrinB2-EphB4 signaling controls bone homeostasis. Cell Metab 2006;4:111–21.
[7] Irie N, Takada Y, Watanabe Y, Matsuzaki Y, Naruse C, Asano M, et al. Bidirectional signaling through ephrinA2-EphA2 enhances osteoclastogenesis and suppresses osteoblastogenesis. J Biol Chem 2009;284:14637–44.
[8] Jaiswal N, Haynesworth SE, Caplan AI, Bruder SP. Osteogenic differentiation of purified, culture-expanded human mesenchymal stem cells in vitro. J Cell Biochem 1997;64:295–312.
[9] Indrawattana N, Chen G, Tadokoro M, Shann LH, Ohgushi H, Tateishi T, et al. Growth factor combination for chondrogenic induction from human mesenchymal stem cell. Biochem Biophys Res Commun 2004;320:914–9.
[10] Torigoe I, Sotome S, Tsuchiya A, Yoshii T, Takahashi M, Kawabata S, et al. Novel cell seeding system into a porous scaffold using a modified low-pressure method to enhance cell seeding efficiency and bone formation. Cell Transplant 2007;16:729–39.
[11] Yoshii T, Sotome S, Torigoe I, Tsuchiya A, Maehara H, Ichinose S, et al. Fresh bone marrow introduction into porous scaffolds using a simple low-pressure loading method for effective osteogenesis in a rabbit model. J Orthop Res 2009;27:1–7.
[12] Chen J, Sotome S, Wang J, Orii H, Uemura T, Shinomiya K. Correlation of in vivo bone formation capability and in vitro differentiation of human bone marrow stromal cells. J Med Dent Sci 2005;52:27–34.
[13] Otaki N, Matsuo K. Bone cell interactions through eph-ephrin: bone modeling, remodeling and associated diseases. Cell Adh Migr 2012;6:148–56.
[14] Bonab MM, Alimoghaddam K, Talebian F, Ghaffari SH, Ghavamzadeh A, Nikbin B. Aging of mesenchymal stem cell in vitro. BMC Cell Biol 2006;7:14.
[15] Digirolamo CM, Stokes D, Colter D, Phinney DG, Class R, Prockop DJ. Propagation and senescence of human marrow stromal cells in culture: a simple colony-forming assay identifies samples with the greatest potential to propagate and differentiate. Br J Haematol 1999;107:275–81.
[16] Oshina H, Sotome S, Yoshii T, Torigoe I, Sugata Y, Maehara H, et al. Effects of continuous dexamethasone treatment on differentiation capabilities of bone marrow-derived mesenchymal cells. Bone 2007;41:575–83.
[17] Osugi M, Katagiri W, Yoshimi R, Inukai T, Hibi H, Ueda M. Conditioned media from mesenchymal stem cells enhanced bone regeneration in rat calvarial bone defects. Tissue Eng Part A 2012;18:1479–89.
[18] Pasquale EB. Eph receptors and ephrins in cancer: bidirectional signalling and beyond. Nat Rev Cancer 2010;10:165–80.
[19] Pasquale EB. Eph-ephrin bidirectional signaling in physiology and disease. Cell 2008;133:38–52.
[20] Pasquale EB. Eph receptor signalling casts a wide net on cell behaviour. Nat Rev Mol Cell Biol 2005;6:462–75.
[21] Schmucker D, Zipursky SL. Signaling downstream of eph receptors and ephrin ligands. Cell 2001;105:701–4.
[22] Noren NK, Yang NY, Silldorff M, Mutyala R, Pasquale EB. Ephrin-independent regulation of cell substrate adhesion by the EphB4 receptor. Biochem J 2009;422:433–42.
[23] Miao H, Wang B. EphA receptor signaling-complexity and emerging themes. Semin Cell Dev Biol 2011;23:16–25.
[24] Abdul-Aziz NM, Turmaine M, Greene ND, Copp AJ. EphrinA–EphA receptor interactions in mouse spinal neurulation: implications for neural fold fusion. Int J Dev Biol 2009;53:559–68.
[25] Akaneya Y, Sohya K, Kitamura A, Kimura F, Washburn C, Zhou R, et al. Ephrin-A5 and EphA5 interaction induces synaptogenesis during early hippocampal development. PLoS One 2010;5:e12486.
[26] Hara Y, Nomura T, Yoshizaki K, Frisen J, Osumi N. Impaired hippocampal neurogenesis and vascular formation in ephrin-A5-deficient mice. Stem Cells 2010;28:974–83.
[27] Holmberg J, Armulik A, Senti KA, Edoff K, Spalding K, Momma S, et al. Ephrin-A2 reverse signaling negatively regulates neural progenitor proliferation and neurogenesis. Genes Dev 2005;19:462–71.
[28] Hornberger MR, Dutting D, Ciossek T, Yamada T, Handwerker C, Lang S, et al. Modulation of EphA receptor function by coexpressed ephrinA ligands on retinal ganglion cell axons. Neuron 1999;22:731–42.
[29] Yue Y, Chen ZY, Gale NW, Blair-Flynn J, Hu TJ, Yue X, et al. Mistargeting hippocampal axons by expression of a truncated eph receptor. Proc Natl Acad Sci U S A 2002;99:10777–82.
[30] Zimmer G, Kastner B, Weth F, Bolz J. Multiple effects of ephrin-A5 on cortical neurons are mediated by SRC family kinases. J Neurosci 2007;27:5643–53.
[31] Miao H, Wei BR, Peehl DM, Li Q, Alexandrou T, Schelling JR, et al. Activation of EphA receptor tyrosine kinase inhibits the Ras/MAPK pathway. Nat Cell Biol 2001;3:527–30.
[32] Tanaka M, Kamata R, Sakai R. EphA2 phosphorylates the cytoplasmic tail of claudin-4 and mediates paracellular permeability. J Biol Chem 2005;280:42375–82.
[33] Ting MC, Wu NL, Roybal PG, Sun J, Liu L, Yen Y, et al. EphA4 as an effector of Twist1 in the guidance of osteogenic precursor cells during calvarial bone growth and in craniosynostosis. Development 2009;136:855–64.
[34] Flenniken AM, Gale NW, Yancopoulos GD, Wilkinson DG. Distinct and overlapping expression patterns of ligands for eph-related receptor tyrosine kinases during mouse embryogenesis. Dev Biol 1996;179:382–401.
[35] Gale NW, Holland SJ, Valenzuela DM, Flenniken A, Pan L, Ryan TE, et al. Eph receptors and ligands comprise two major specificity subclasses and are reciprocally compartmentalized during embryogenesis. Neuron 1996;17:9–19.
[36] Wang HU, Chen ZF, Anderson DJ. Molecular distinction and angiogenic interaction between embryonic arteries and veins revealed by ephrin-B2 and its receptor eph-B4. Cell 1998;93:741–53.
[37] Alam SM, Fujimoto J, Jahan I, Sato E, Tamaya T. Coexpression of EphB4 and ephrinB2 in tumour advancement of ovarian cancers. Br J Cancer 2008;98:845–51.
[38] Astin JW, Batson J, Kadir S, Charlet J, Persad RA, Gillatt D, et al. Competition amongst eph receptors regulates contact inhibition of locomotion and invasiveness in prostate cancer cells. Nat Cell Biol 2010;12:1194–204.
[39] Dong Y, Wang J, Sheng Z, Li G, Ma H, Wang X, et al. Downregulation of EphA1 in colorectal carcinomas correlates with invasion and metastasis. Mod Pathol 2009;22:151–60.

[40] Fu DY, Wang ZM, Wang BL, Chen L, Yang WT, Shen ZZ, et al. Frequent epigenetic inactivation of the receptor tyrosine kinase EphA5 by promoter methylation in human breast cancer. Hum Pathol 2010;41:48–58.
[41] Hahn AS, Kaufmann JK, Wies E, Naschberger E, Panteleev-Ivlev J, Schmidt K, et al. The ephrin receptor tyrosine kinase A2 is a cellular receptor for Kaposi's sarcoma-associated herpesvirus. Nat Med 2012;18:961–6.
[42] Herath NI, Boyd AW. The role of eph receptors and ephrin ligands in colorectal cancer. Int J Cancer 2010;126:2003–11.
[43] Wang B. Cancer cells exploit the eph-ephrin system to promote invasion and metastasis: tales of unwitting partners. Sci Signal 2011;4:pe28.
[44] Almog N, Ma L, Raychowdhury R, Schwager C, Erber R, Short S, et al. Transcriptional switch of dormant tumors to fast-growing angiogenic phenotype. Cancer Res 2009;69:836–44.
[45] Dobrzanski P, Hunter K, Jones-Bolin S, Chang H, Robinson C, Pritchard S, et al. Antiangiogenic and antitumor efficacy of EphA2 receptor antagonist. Cancer Res 2004;64:910–9.
[46] Sharfe N, Nikolic M, Cimpeon L, Van De Kratts A, Freywald A, Roifman CM. EphA and ephrin-A proteins regulate integrin-mediated T lymphocyte interactions. Mol Immunol 2008;45:1208–20.
[47] Lin CC, Anseth KS. Cell–cell communication mimicry with poly(ethylene glycol) hydrogels for enhancing beta-cell function. Proc Natl Acad Sci U S A 2011;108:6380–5.
[48] Konstantinova I, Nikolova G, Ohara-Imaizumi M, Meda P, Kucera T, Zarbalis K, et al. EphA-ephrin-A-mediated beta cell communication regulates insulin secretion from pancreatic islets. Cell 2007;129:359–70.
[49] Negishi-Koga T, Shinohara M, Komatsu N, Bito H, Kodama T, Friedel RH, et al. Suppression of bone formation by osteoclastic expression of semaphorin 4D. Nat Med 2011;17:1473–80.
[50] Hayashi M, Nakashima T, Taniguchi M, Kodama T, Kumanogoh A, Takayanagi H. Osteoprotection by semaphorin 3A. Nature 2012;485:69–74.
[51] Allan EH, Hausler KD, Wei T, Gooi JH, Quinn JM, Crimeen-Irwin B, et al. EphrinB2 regulation by PTH and PTHrP revealed by molecular profiling in differentiating osteoblasts. J Bone Miner Res 2008;23:1170–81.
[52] Kuroda C, Kubota S, Kawata K, Aoyama E, Sumiyoshi K, Oka M, et al. Distribution, gene expression, and functional role of EphA4 during ossification. Biochem Biophys Res Commun 2008;374:22–7.
[53] Huai J, Drescher U. An ephrin-A-dependent signaling pathway controls integrin function and is linked to the tyrosine phosphorylation of a 120-kDa protein. J Biol Chem 2001;276:6689–94.
[54] Yamazaki T, Masuda J, Omori T, Usui R, Akiyama H, Maru Y. EphA1 interacts with integrin-linked kinase and regulates cell morphology and motility. J Cell Sci 2009;122:243–55.
[55] Julich D, Mould AP, Koper E, Holley SA. Control of extracellular matrix assembly along tissue boundaries via integrin and Eph/Ephrin signaling. Development 2009;136:2913–21.
[56] Hamidouche Z, Fromigue O, Ringe J, Haupl T, Vaudin P, Pages JC, et al. Priming integrin alpha5 promotes human mesenchymal stromal cell osteoblast differentiation and osteogenesis. Proc Natl Acad Sci U S A 2009;106:18587–91.

Spine

SPINE Volume 38, Number 10, pp 833–840

CERVICAL SPINE

Porous/Dense Composite Hydroxyapatite for Anterior Cervical Discectomy and Fusion

Toshitaka Yoshii, MD, PhD,*† Masato Yuasa, MD,*† Shinichi Sotome, MD, PhD,*† Tsuyoshi Yamada, MD,*† Kyohei Sakaki, MD,* Takashi Hirai, MD,*† Takashi Taniyama, MD,*† Hiroyuki Inose, MD, PhD,*† Tsuyoshi Kato, MD, PhD,* Yoshiyasu Arai, MD, PhD,* Shigenori Kawabata, MD, PhD,* Shoji Tomizawa, MD, PhD,* Mitsuhiro Enomoto, MD, PhD,*† Kenichi Shinomiya, MD, PhD,*†‡ and Atsushi Okawa, MD, PhD*†‡

Study Design. A prospective analysis

Objective. Our aim was to investigate the efficacy of new synthetic porous/dense composite hydroxyapatite (HA) for use in anterior cervical discectomy and fusion (ACDF).

Summary of Background Data. Iliac crest bone graft (ICBG) has been traditionally used as the "gold standard" for ACDF. The significant complication rate associated with harvesting tricortical ICBG, however, has encouraged development of alternative graft substitutes.

Methods. The morphology of the porous/dense HA was observed by scanning electron microscopy (SEM), and the *in vitro* compressive strength of the composite HA was measured. From April 2005, 51 consecutive patients underwent 81 levels of ACDF using the composite HA with percutaneously harvested trephine bone chips. Clinical and radiological evaluation was performed during the postoperative hospital stay and at follow-up. Furthermore, the outcomes in ACDF using the composite HA were compared with those using tricortical ICBG.

Results. The SEM images demonstrated 100- to 300-μm pores (approximately 40% of porosity) in the porous layers of the HA. The compressive strength of the composite HA was 203.1 ± 4.1 MPa. In the clinical study, the demographic data of the patients were similar in HA and ICBG groups. The fusion rates in HA group were comparable with those in ICBG group. The cervical lordosis was enhanced postoperatively in both groups and well preserved at 2-year follow-up without significant differences between the groups. The intraoperative blood loss in HA group was significantly lesser than that in ICBG group. Donor site complications were found in 29.2% of the patients in ICBG group, whereas no donor site morbidity was found in HA group. No major collapse or fragmentation of the composite HA was found.

Conclusion. The hybrid graft of composite HA and percutaneously harvested trephine chips seemed promising as a graft substitute for ACDF.

Key words: anterior cervical discectomy and fusion, graft substitute, hydroxyapatite, donor site morbidity.

Level of Evidence: 4

Spine 2013;38:833–840

Anterior cervical discectomy and fusion (ACDF) is a widely accepted treatment of cervical disc diseases.[1,2] As a common practice, autologous tricortical strut bone harvested from the iliac crest has been used for ACDF.[2,3] There are, however, significant complications at the donor site with this method, including donor site pain, hematoma, infection, fracture of the ilium, sensory disturbance, and cosmetic disability.[4] In addition, the rate of complications is known to be higher in anterior harvest from the iliac crest than in posterior harvest.[5] Because of the morbidity associated with autograft harvesting, alternative graft materials for ACDF have been developed.[6–8]

Hydroxyapatite (HA), a highly crystalline form of calcium phosphate, is a biocompatible ceramic produced by a high-temperature reaction. The nominal composition of this mixture is $Ca_{10}(PO_4)_6(OH)_2$, with a calcium-to-phosphate atomic ratio of 1.67. The unique property of this material is its chemical similarity with the mineralized phase of the bone; this similarity accounts for its osteoconductive potential and excellent biocompatibility.[9,10] HA blocks have been investigated as a graft substitute for ACDF.[11–15] Different preparative methods of HA can lead to either a dense or porous structure. Although greater porosity of the material enhances interface activity and bone ingrowth, its brittle mechanical property possesses low resistance against fracture.[15,16] In HA blocks with a dense structure, more crystallization and higher density result in greater mechanical strength. However, the interface

From the *Section of Orthopaedic and Spinal Surgery, Graduate School; †Section of Regenerative Therapeutics for Spine and Spinal Cord, Graduate School, and ‡Global Center of Excellence (GCOE) Program for International Research Center for Molecular Science in Tooth and Bone Disease, Tokyo Medical and Dental University, Tokyo, Japan.

Acknowledgment date: July 18, 2012. Revision date: October 11, 2012. Acceptance date: November 17, 2012.

The device(s)/drug(s) is/are FDA approved or approved by corresponding national agency for this indication.

No funds were received in support of this work.

Relevant financial activities outside the submitted work: grants.

Address correspondence and reprint requests to Toshitaka Yoshii, MD, PhD, Department of Orthopaedic and Spinal Surgery, Graduate School, Tokyo Medical and Dental University, 1-5-45 Yushima, Bunkyo-ku, Tokyo, 113-8519, Japan; E-mail: yoshii.orth@tmd.ac.jp

DOI: 10.1097/BRS.0b013e3182801390

activity between the material and the host bone is lower than the porous HA blocks.[12,17,18]

Given these problems, we devised a new synthetic HA block with a unique composite structure: a dense layer at the center for load bearing and porous layers on the sides of the material. In this study, we investigated both the *in vitro* mechanical properties and the *in vivo* efficacy of the composite HA for use in ACDF. To enhance interbody fusion, we used the composite HA with percutaneously harvested small cancellous chips (trephine bone).[19] The outcomes of ACDF using this hybrid graft were compared with a historical control group of patients who underwent ACDF using an autologous tricortical strut of iliac crest bone graft (ICBG). This study was approved by an institutional review board.

MATERIALS AND METHODS

Material Preparation, Scanning Electron Microscopy, and Mechanical Properties

To synthesize the HA, an aqueous solution of H_3PO_4 was added to an aqueous solution of $Ca(OH)_2$. Subsequently, the dried powder of apatite was compressed into a mold, and a multilayer block was prepared in the following manner without any adhesive agents. First, the apatite powder was mixed with the pore-forming material and added to a mold (porous layer). Then, apatite powder was layered on the porous layer without pore openers (dense layer). Apatite powder mixed with the pore-forming material was further layered on the compact layer. Finally, the 3-layered apatite was compressed and sintered at approximately 1150°. The synthesized HA for ACDF (Boneceram; Olympus Terumo Biomaterials Corp., Tokyo, Japan) is wedge-shaped: the anterior height was 1 or 2 mm higher than the posterior height. The morphology of the composite HA was observed by scanning electron microscopy (SEM). The composite HA samples were mounted on an SEM pin stub mount and sputter-coated with gold. A S-2600H scanning electron microscope (Hitachi, Tokyo, Japan) was used to acquire images. The pore size of the porous layer was assessed using SEM images of triplicate samples. The density of the porous layer of the HA block was determined from the mass and volume measurements of the triplicate samples. The porosity was subsequently calculated from the known density of HA (3.1 g/cm^3).[20] To measure the compressive mechanical strength of the composite HA, samples of composite HA were placed between 2 fixed compression platens of a mechanical testing device (AUTO GRAPH 2000GE) and loaded at 0.5 mm min^{-1} until failure.

ACDF Using Porous/Dense Composite HA

From April 2005 to July 2009, 51 consecutive patients (41 males and 10 females, average age of 53.0 yr) underwent 81 levels of ACDF using the porous/dense composite HA with trephine chips in our institution after providing the appropriate informed consent. The principal diagnoses were as follows: cervical disc herniation: 20, cervical spondylotic myelopathy: 21, cervical spondylotic amyotrophy: 9, and ossification of posterior longitudinal ligament: 1. We performed single-level fusion in 29 patients and multilevel fusion in 22 patients (2-level: 14, 3-level: 8 patients) (Table 1).

Surgical Procedures

A standard Smith–Robinson approach to the cervical spine was used.[2] A discectomy was performed after confirmation and exposure of the appropriate vertebral levels. A high-speed burr was used to remove the cartilaginous endplates from the adjoining vertebral bodies; excessive removal of the subchondral bone was avoided. After decompression, the composite HA blocks were inserted into the intervertebral spaces. There are various sizes of the composite HA blocks (width: 11 mm; length: 12 mm; anterior height: 7, 8, or 9 mm). The size of the HA block was determined by measuring the height of the intervertebral space and was verified using a trial spacer. Subsequently, rod-shaped autologous cancellous bone sticks were percutaneously harvested from the anterior iliac crest using an 8-gauge Jamshidi biopsy needle (Figure 1A).[19] After 4 to 5 sticks per level (length: 10 mm) were harvested, we grafted the cancellous sticks beside the HA block (between the porous layers of the HA block and Lushka joints) to further enhance the interbody fusion (Figure 1B). After hybrid grafting of the composite HA with trephine bone chips, anterior plating (Atlantis Plate, Medtronic Sofamor Danek, Memphis, TN) was performed. A neck collar was used for 3 months after surgery. The patients had follow-up examinations at 3, 6, and 12 months after surgery and yearly thereafter. All patients were followed for a minimum of 2 years.

TABLE 1. Patient Demographic Data

	HA	ICBG
N	51	24
Age (yr) (mean ± SD)	53.0 ± 11.0	58.1 ± 13.5
Sex: Male/female	41/10	16/8
Pre-JOA score (mean ± SD)	12.0 ± 2.5	11.1 ± 2.8
Smoking	23/51	7/24
Follow-up (mo) (mean ± SD)	38.5 ± 15.9	83.8 ± 7.0*
Levels	81	41
1-level	29	11
2-level	14	9
3-level	8	4
Disease		
CDH	20	6
CSM	21	14
CSA	9	2
OPLL	1	2

*$P < 0.001$.

HA indicates hydroxyapatite; ICBG, iliac crest bone graft; JOA, Japanese Orthopaedics Association; CDH, cervical disc herniation; CSM, cervical spondylotic myelopathy; CSA, cervical spondylotic amyotrophy; OPLL, ossification of posterior longitudinal ligament.

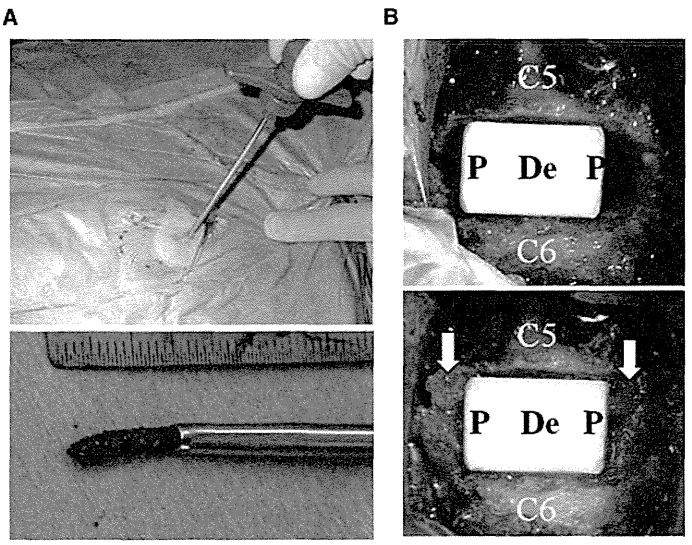

Figure 1. **(A)** rod-shaped autologous cancellous bone sticks were percutaneously harvested from the anterior iliac crest using an 8-gauge Jamshidi biopsy needle. **(B)** The harvested cencellous bone sticks (trephine bone: white arrows) were grafted on the lateral sides of the hydroxyapatite (HA) block (between the porous layers of the composite HA and Lushka joints).

Clinical Outcomes

Neurological functions were evaluated using a Japanese Orthopaedic Association (JOA) scoring and its recovery rate.[21] In addition, operation time, intraoperative bleeding, and postoperative complications were evaluated.

Radiographical Outcomes

Plain anteroposterior and lateral cervical spine radiographs were obtained before and after surgery and at each follow-up examination. The Cobb angle was measured between the upper and lower vertebrae in the motion segment subjected to the surgery. The cervical sagittal lordosis was evaluated between C2 and C7. The fusion status was assessed by 2 independent spine surgeons. The radiographical fusion criteria were as follows: (1) the absence of a radiolucent zone between the HA and the endplates on the reconstructed computed tomographic (CT) scans, (2) continuous bone bridging across the intervertebral space on the lateral sides of the HA block on reconstructed CT scans, and (3) the lack of translation or angulation change in the lateral flexion–extension radiographs. A successful fusion was defined when both observers agreed that these findings were present.

The clinical and radiological outcomes of ACDF using the HA blocks with trephine chips (HA group) were compared with those of a historical control group of 24 patients (16 males and 8 females, average age, 58.1 yr) who underwent 41 levels of ACDF using an autologous tricortical strut of ICBG and anterior plating in our institution from 2003 to 2004 (ICBG group) (Table 1). In the ICBG group, we harvested an appropriately sized tricortical autologous graft (approximately 7–9 mm in height) from the anterior iliac crest. We generally reconstructed the defect in the iliac crest using a porous β-tricalcium phosphate spacer (Osferion; Olympus Terumo Biomaterials Corp., Tokyo, Japan). Statistical analyses were performed using an unpaired t test for continuous variables, a Mann-Whitney U test for discontinuous variables, and a χ^2 test for categorical data. The significance level was set to $P < 0.05$.

RESULTS

Scanning Electron Microscopy, Mechanical Properties

SEM images of the composite HA are shown in Figure 1. The porous layer at the sides of the composite HA was approximately 1-mm wide (Figures 2A, B). The porosity was approximately 40%, and the pore size was in the range of 100 to 300 μm in diameter (Figure 2C). The mechanical testing revealed that the compressive strength of the composite HA was 203.1 ± 4.1 MPa (Figure 2D).

Clinical and Radiographical Outcomes in ACDF

The demographic data of the patients in the HA and ICBG groups were similar. There were no significant differences in age, sex, diseases, number of treated levels during surgery, or preoperative neurological function based on the JOA score. There was a significant difference between the 2 groups in the follow-up length.

The neurological scores were significantly improved ($P < 0.05$) after surgery in both groups (Table 2). There were no significant differences between the 2 groups in the postoperative recovery rate based on JOA score (66.1% in the HA group and 57.4% in the ICBG group).

Figure 3 shows representative postoperative CT scans in a case with successful fusion and a case with nonunion. In case 1, the CT scan obtained just after surgery shows that the small trephine bone chips were grafted onto the sides of the composite HA (Figure 3A). Two years postoperatively, successful fusion was confirmed at both the C4–C5 and C 5–C6 levels on the reconstructed CT scan. Continuous bone bridging across the intervertebral space on the lateral sides of HA was observed without a radiolucent zone between the HA and the endplates (Figure 3A). For patient in case 2, the C5–C6 level was judged as a nonunion. An obvious radiolucent zone between the HA and the lower endplate was observed, and the lateral bone bridging was not completed on the CT scans obtained 2 years postoperatively (Figure 3B).

The ACDF using HA achieved successful fusion in 47 of 51 cases: 100% (29/29) in single-level, 85.7% (12/14) in 2-level, and 75.0% (6/8) in 3-level surgical procedures. These fusion rates in the HA group were comparable with those in the ICBG group: 100% (11/11) in single-level, 88.9% (8/9) in 2-level, and 75.0% (3/4) in 3-level ACDF (Table 3). There were no significant differences in the fusion rates between the 2 groups. The segmental lordosis at the fused segments was enhanced postoperatively in both the HA and ICBG groups and well preserved at the 2-year follow-up (Figure 4A). However, the postoperative improvement in the lordotic angle was not significantly different between the 2 groups (Figure 4B). A similar result was observed in the cervical alignment at C2–C7. The cervical alignment was enhanced after surgery and preserved

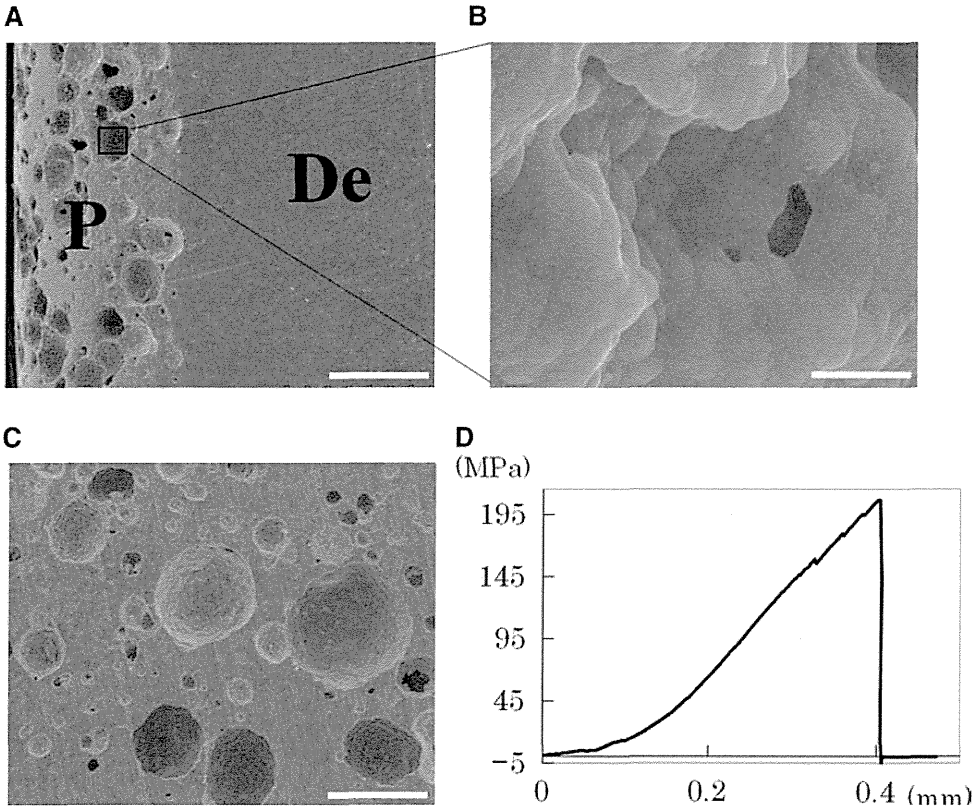

Figure 2. **(A)** Scanning electron microscopy analysis of the composite hydroxyapatite (HA). Scale bar: 500 μm. **(B)** High magnification of the porous layer. Scale bar: 2.5 μm. **(C)** The surface of the porous layer of the composite HA. Scale bar: 250 μm. **(D)** Compressive strength of the composite HA. P indicates porous layer; De, dense layer.

at the 2-year follow-up in both groups (Figure 4C). However, the changes in the lordotic angle at C2–C7 were not significantly different between the groups (Figure 4D).

The operation time tended to be shorter in the HA group; however, this difference was not significant (Figure 5A). The intraoperative blood loss in the HA group was significantly lower ($P < 0.05$) than that in the ICBG group in both single- and multilevel fusions (Figure 5B). The incidence of postoperative complications was similar in the HA group (dysphagia: 2, esophageal perforation: 1, C5 palsy: 1) and the ICBG group (dysphagia: 1, C5 palsy: 1). However, there were significant differences in the occurrence of donor site complications; 29.2% (7/24) of patients in the ICBG group complained of prolonged pain or sensory disturbance at the donor site, whereas no donor site morbidity was reported in the HA group. Minor cracks of the graft were found at the corner of the porous layer in 4 HA blocks (4.9%) on postoperative radiographs and CT scans obtained immediately after the surgical procedures, suggesting that the cracks occurred at the time of insertion. No cracks were found in the center portion (the dense layer), which bears most of the load. These cracks did not affect the stability or alignment of the operated segments, and all of these cases eventually achieved radiographical fusion.

TABLE 2. Neurological Outcomes

	HA (mean ± SD)	ICBG (mean ± SD)
Pre-operation	12.0 ± 2.5	11.1 ± 2.9
Postoperation (2y)	15.0 ± 1.3	14.5 ± 1.6
IR (%)	66.1 ± 24.5	57.4 ± 15.6

HA indicates hydroxyapatite; ICBG, iliac crest bone graft; IR, improvement rate.

DISCUSSION

The goals of ACDF include pain relief, removal of neural compression, restoration of stability, and restoration or maintenance of disc height, foraminal space, and spinal alignment.[22–25] An autologous tricortical graft harvested from the iliac crest can provide satisfactory clinical results in achieving these goals.[26] However, the high rate of donor site complications has motivated spinal surgeons to seek alternative materials to avoid harvesting iliac bone grafts.[5,6] Fibula allograft is considered to be an excellent option, but the union rate is not as high as with iliac autograft.[26] Furthermore, this allograft is not commercially available in some Asian countries, including Japan, and thus is rarely used in ACDF. Other options include titanium or polyetheretherketone cages, polymethylmethacrylate, and an osteoconductive ceramic spacer such as HA.[6,14,15,27,28]

HA, a highly crystalline form of calcium phosphate, is a biocompatible ceramic produced by a high-temperature reaction. Since synthetic techniques of producing HA were established, synthetic HA has been extensively used clinically for bone defects and spinal fusion.[6,12,15,29] Generally, a high porosity of synthetic HA exposes a large surface area to the host tissue. As a result, it can provide a better scaffold

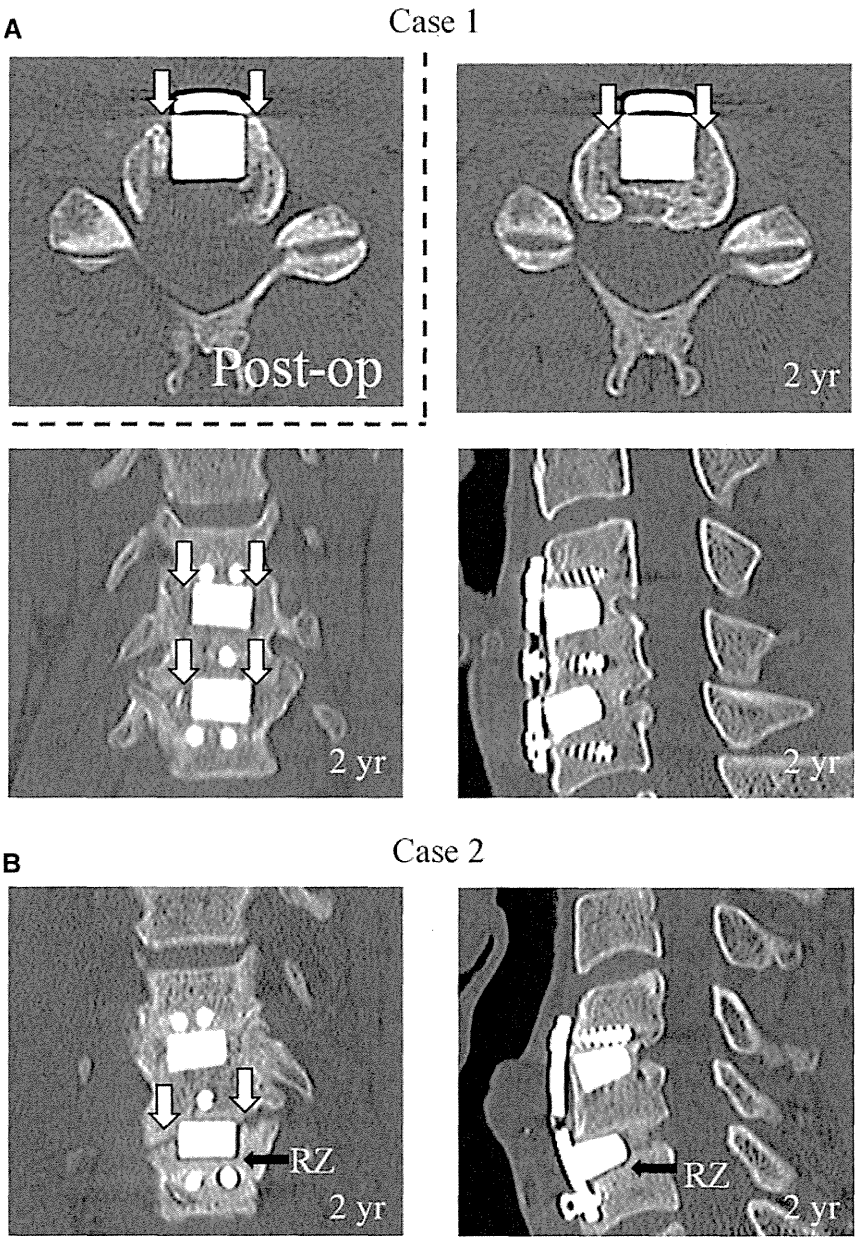

Figure 3. (A) Case 1: C4–C5, C5–C6 anterior cervical discectomy and fusion (ACDF) (51-yr-old male) with successful fusion. Upper left: Computed tomographic scan obtained immediately after ACDF using the hybrid graft. A successful fusion was confirmed both at C4–C5 and C5–C6 levels on the CT scans 2 years postoperatively (2 yr). White arrows: trephine bone grafting on the lateral sides of the composite hydroxyapatite. **(B)** Case 2: C4–C5, C5–C6 ACDF (49-yr-old male) with nonunion. In the CT scans 2 years after ACDF, radiolucent zone (RZ: black arrows) and lack of the continuous lateral bone bridging (white arrows) were recognized at C5–C6 level.

for osteoblasts and their precursor cells and thus promote biological changes, such as cellular attachment and bone formation. However, the porous structure is known to be associated with lower mechanical properties and less initial strength after implantation.[12,18]

Previously, Zdeblick *et al*[15] have reported a high collapse rate of coralline-derived porous HA in a dog interbody fusion model, although the fusion rate was acceptable. McConnell *et al*[11] have compared porous coralline HA and ICBG as a graft material for ACDF. Their studies have demonstrated much higher rates of graft fragmentation in porous HA than in ICBG, while the fusion rates are similar between HA and ICBG. In contrast, a dense HA has a greater mechanical strength and is associated with a small rate of graft collapse when used in ACDF.[30] However, the osteoconductivity of dense HA is lower than the porous HA because there is less interaction between the material and the host bone.[12,17,18] To achieve a more reliable interbody fusion, it is desirable that the material possess both sufficient osteoconductive properties and mechanical strength.

TABLE 3. Radiographical Fusion Rates

	HA	ICBG
1-level	29/29 (100%)	11/11 (100%)
2-level	12/14 (85.7%)	8/9 (88.9%)
3-level	6/8 (75.0%)	3/4 (75.0%)

HA indicates hydroxyapatite; ICBG, iliac crest bone graft.

The composite HA used in this study consists of 3 layers: a dense layer at the center and porous layers on both sides of the material. SEM analysis revealed that the porous layer has a highly porous structure, which can enhance interface

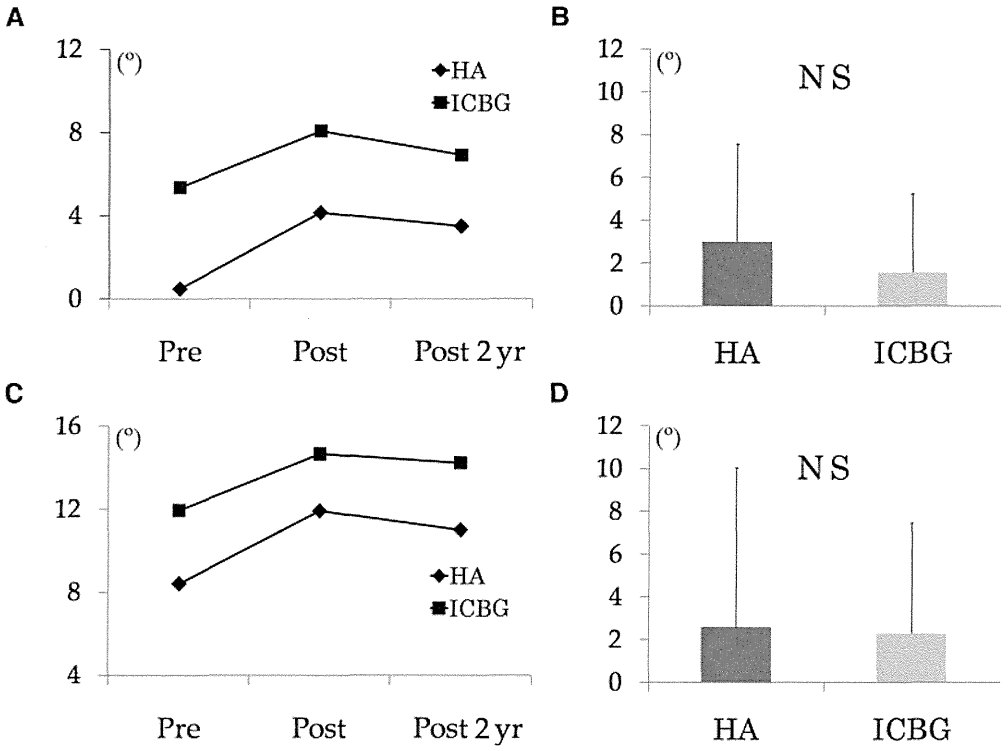

Figure 4. Lordosis at the fused segments **(A)** and at C2–C7 **(C)** at preoperative (pre), postoperative (post), and postoperative 2-year (post 2 yr) time points. The postoperative improvement of lordosis at the fused segments **(B)** and at C2–C7 **(D)**. NS indicates not significant; HA, hydroxyapatite; ICBG, iliac crest bone graft.

activity and osseous ingrowth. In this study, we grafted percutaneously harvested trephine bone chips on the sides of the material to enhance the bridging of the interbody space and further promote interface osteogenesis between the porous layers and the host bone. In the postoperative CT scans, fusion was observed at both the center part (between the HA and vertebrae) and the lateral part in most cases (47/51), suggesting that both the HA and the trephine cancellous sticks contribute to the fusion. The successful fusion rates in ACDF using this hybrid graft were similar to the fusion rates in ACDF using ICBG in this study and in previous studies.[31,32] From these results, the composite HA has sufficient osteoconductive properties for interbody fusion when used with the small trephine chips.

Several studies have investigated the biomechanical strength required for ACDF and reported that the normal compressive load on the graft ranges from 12 to 90 N.[33,34] In this study, mechanical testing demonstrated that the composite HA has a compressive strength of approximately 200 MPa (>20 kN), which is stronger than tricortical ICBG,[35] and is thought to have sufficient mechanical strength for load bearing. However, there are still potential risks for material collapse caused by repetitive mechanical stress on the graft, as previously reported.[11,16] Because the anterior plating system can reduce mechanical stress on the graft in ACDF,[34] we used anterior plates to minimize the risk of graft failure. There were no cases with major fragmentation or collapse of the composite HA that required revision surgical procedures. The lordosis in the operated segments was significantly enhanced postoperatively and maintained during follow-up periods. Loss of cervical alignment due to hardware failure was not observed in any of the cases. These findings also support the biomechanical stability and reliability of the composite HA for use in ACDF.

In this study comparing the composite HA and ICBG as graft materials for ACDF, no significant differences were found in terms of neurological recovery, fusion rates, or sagittal alignment of the operated segments and cervical spine. The composite HA is wedge-shaped and therefore was expected to enhance the sagittal alignment more than the parallel

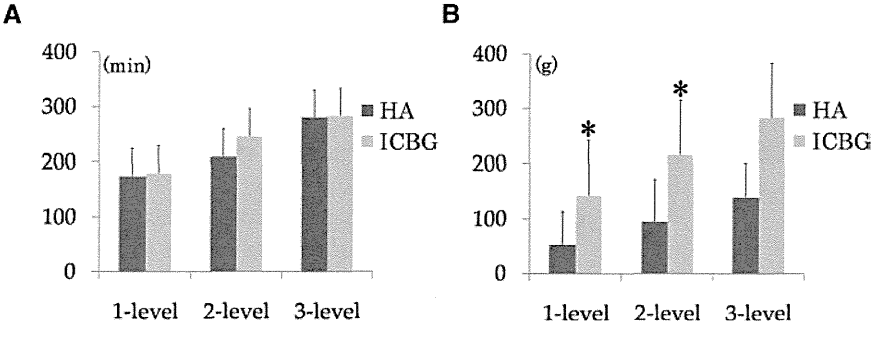

Figure 5. Operating time **(A)** and intraoperative bleeding **(B)** in the HA and ICBG groups. HA indicates hydroxyapatite; ICBG, iliac crest bone graft; $*P < 0.05$ (HA *vs.* ICBG).

tricortical ICBG. However, as previously reported, the shape of the graft in ACDF may not significantly influence postoperative spinal alignment.[36] In the HA group, the operation time was shorter, and the intraoperative blood loss was less than that in the ICBG group for both single-level and multilevel ACDF. The percutaneous harvest of iliac cancellous chips requires a shorter harvesting time with less blood loss than the conventional harvesting method of tricortical ICBG. This percutaneous trephine method is thought to contribute to the reduction in operating time and intraoperative blood loss. The incidence of major complications was similar in the HA and ICBG groups. However, there were significant differences in the occurrence of donor site complications. Notably, no donor site complications were observed in the HA group. These results suggest that ACDF using the hybrid graft is a less invasive method with less intraoperative bleeding and no donor site complications.

There are some limitations in this study. This study compared the composite HA with ICBG as a graft material in ACDF using prospectively collected patient data. However, the comparison was not based on the randomized controlled clinical trial. We did not directly compare the composite HA used in this study with other previously reported HA blocks. We did not compare the hybrid graft composed of the composite HA/trephine chips with the composite HA alone. To fully show the efficacy of the composite HA for use in ACDF, these comparisons may need to be made in the future. Despite these limitations, this study demonstrates that hybrid grafting using the composite HA combined with trephine cancellous chips is a safe and effective alternative procedure to conventional autologous tricortical iliac grafts for ACDF.

➢ Key Points

- ❑ A new synthetic porous/dense HA was developed for ACDF.
- ❑ The composite HA has a sufficient compressive strength for use in ACDF.
- ❑ ACDF using a hybrid graft of the composite HA with percutaneously harvested trephine chips showed similar neurological and radiological outcomes to ACDF using tricortical bone graft (ICBG).
- ❑ ACDF using the hybrid graft demonstrated a successful fusion rate, with less intraoperative bleeding and without donor site complications.

Acknowledgments

The porous/dense composite hydroxyapatite was developed in collaboration with Olympus Terumo Biomaterials Corp. The authors thank Emiko Ueno for her kind support in scanning electron microscopy and mechanical testing. This study was approved by an institutional review board.

References

1. Cloward RB. The anterior approach for removal of ruptured cervical disks. *J Neurosurg* 1958;15:602–17.
2. Smith GW, Robinson RA. The treatment of certain cervical-spine disorders by anterior removal of the intervertebral disc and interbody fusion. *J Bone Joint Surg Am* 1958;40-A:607–24.
3. Floyd T, Ohnmeiss D. A meta-analysis of autograft versus allograft in anterior cervical fusion. *Eur Spine J* 2000;9:398–403.
4. Banwart JC, Asher MA, Hassanein RS. Iliac crest bone graft harvest donor site morbidity. A statistical evaluation. *Spine (Phila Pa 1976)*. 1995;20:1055–60.
5. Ahlmann E, Patzakis M, Roidis N, et al. Comparison of anterior and posterior iliac crest bone grafts in terms of harvest-site morbidity and functional outcomes. *J Bone Joint Surg Am* 2002; 84-A:716–20.
6. Chau AM, Mobbs RJ. Bone graft substitutes in anterior cervical discectomy and fusion. *Eur Spine J* 2009;18:449–64.
7. Jacobs W, Willems PC, Kruyt M, et al. Systematic review of anterior interbody fusion techniques for single- and double-level cervical degenerative disc disease. *Spine (Phila Pa 1976)* 2011;36:E950–60.
8. Ryken TC, Heary RF, Matz PG, et al. Techniques for cervical interbody grafting. *J Neurosurg Spine* 2009;11:203–20.
9. Ghosh SK, Nandi SK, Kundu B, et al. In vivo response of porous hydroxyapatite and beta-tricalcium phosphate prepared by aqueous solution combustion method and comparison with bioglass scaffolds. *J Biomed Mater Res B Appl Biomater* 2008;86:217–27.
10. Nandi SK, Roy S, Mukherjee P, et al. Orthopaedic applications of bone graft & graft substitutes: a review. *Indian J Med Res* 2010;132:15–30.
11. McConnell JR, Freeman BJ, Debnath UK, et al. A prospective randomized comparison of coralline hydroxyapatite with autograft in cervical interbody fusion. *Spine (Phila Pa 1976)* 2003;28:317–23.
12. Spivak JM, Hasharoni A. Use of hydroxyapatite in spine surgery. *Eur Spine J* 2001;10(suppl 2):S197–204.
13. Suetsuna F, Yokoyama T, Kenuka E, et al. Anterior cervical fusion using porous hydroxyapatite ceramics for cervical disc herniation. a two-year follow-up. *Spine J* 2001;1:348–57.
14. Thalgott JS, Fritts K, Giuffre JM, et al. Anterior interbody fusion of the cervical spine with coralline hydroxyapatite. *Spine (Phila Pa 1976)* 1999;24:1295–9.
15. Zdeblick TA, Cooke ME, Kunz DN, et al. Anterior cervical discectomy and fusion using a porous hydroxyapatite bone graft substitute. *Spine (Phila Pa 1976)* 1994;19:2348–57.
16. Ito M, Abumi K, Shono Y, et al. Complications related to hydroxyapatite vertebral spacer in anterior cervical spine surgery. *Spine (Phila Pa 1976)* 2002;27:428–31.
17. Nishikawa M, Myoui A, Ohgushi H, et al. Bone tissue engineering using novel interconnected porous hydroxyapatite ceramics combined with marrow mesenchymal cells: quantitative and three-dimensional image analysis. *Cell Transplant* 2004;13:367–76.
18. Yoshikawa H, Myoui A. Bone tissue engineering with porous hydroxyapatite ceramics. *J Artif Organs* 2005;8:131–6.
19. Yamada T, Yoshii T, Sotome S, et al. Hybrid grafting using bone marrow aspirate combined with porous beta-tricalcium phosphate and trephine bone for lumbar posterolateral spinal fusion: a prospective, comparative study versus local bone grafting. *Spine (Phila Pa 1976)* 2012;37:E174–9.
20. Wagh AS. Chemically Bonded Phosphate Ceramics: Twenty-first Century Materials With Diverse Applications. Amsterdam, Netherlands: Elsevier Science; 2004.
21. Dai LY, Jiang LS. Single-level instrumented posterolateral fusion of lumbar spine with beta-tricalcium phosphate versus autograft: a prospective, randomized study with 3-year follow-up. *Spine (Phila Pa 1976)* 2008;33:1299–1304.
22. Anakwenze OA, Auerbach JD, Milby AH, et al. Sagittal cervical alignment after cervical disc arthroplasty and anterior cervical discectomy and fusion: results of a prospective, randomized, controlled trial. *Spine (Phila Pa 1976)* 2009;34:2001–7.
23. Bartels RH, Donk R, van Azn RD. Height of cervical foramina after anterior discectomy and implantation of a carbon fiber cage. *J Neurosurg* 2001;95(suppl):40–2.
24. Bohlman HH, Emery SE, Goodfellow DB, et al. Robinson anterior cervical discectomy and arthrodesis for cervical radiculopathy. Long-term follow-up of one hundred and twenty-two patients. *J Bone Joint Surg Am* 1993;75:1298–307.

25. Simmons EH, Bhalla SK. Anterior cervical discectomy and fusion. A clinical and biomechanical study with eight-year follow-up. *J Bone Joint Surg Br* 1969;51:225–37.
26. Bishop RC, Moore KA, Hadley MN. Anterior cervical interbody fusion using autogeneic and allogeneic bone graft substrate: a prospective comparative analysis. *J Neurosurg* 1996;85:206–10.
27. Barlocher CB, Barth A, Krauss JK, et al. Comparative evaluation of microdiscectomy only, autograft fusion, polymethylmethacrylate interposition, and threaded titanium cage fusion for treatment of single-level cervical disc disease: a prospective randomized study in 125 patients. *Neurosurg Focus* 2002;12:E4.
28. Liao JC, Niu CC, Chen WJ, et al. Polyetheretherketone (PEEK) cage filled with cancellous allograft in anterior cervical discectomy and fusion. *Int Orthop* 2008;32:643–8.
29. Shibuya K, Kurosawa H, Takeuchi H, Niwa S. The medium-term results of treatment with hydroxyapatite implants. *J Biomed Mater Res B Appl Biomater* 2005;75:405–13.
30. Senter HJ, Kortyna R, Kemp WR. Anterior cervical discectomy with hydroxylapatite fusion. *Neurosurgery* 1989;25:39–42; discussion 42–3.
31. Suchomel P, Barsa P, Buchvald P, et al. Autologous versus allogenic bone grafts in instrumented anterior cervical discectomy and fusion: a prospective study with respect to bone union pattern. *Eur Spine J* 2004;13:510–5.
32. Samartzis D, Shen FH, Goldberg EJ, et al. Is autograft the gold standard in achieving radiographic fusion in one-level anterior cervical discectomy and fusion with rigid anterior plate fixation? *Spine (Phila Pa 1976)* 2005;30:1756–61.
33. Olsewski JM, Garvey TA, Schendel MJ. Biomechanical analysis of facet and graft loading in a Smith-Robinson type cervical spine model. *Spine (Phila Pa 1976)* 1994;19:2540–4.
34. Rapoff AJ, O'Brien TJ, Ghanayem AJ, et al. Anterior cervical graft and plate load sharing. *J Spinal Disord* 1999;12:45–9.
35. Smith MD, Cody DD. Load-bearing capacity of corticocancellous bone grafts in the spine. *J Bone Joint Surg Am* 1993;75:1206–13.
36. Villavicencio AT, Babuska JM, Ashton A, et al. Prospective randomized double blinded clinical study evaluating the correlation of clinical outcomes and cervical sagittal alignment. *Neurosurgery* 2011;68:1309–16.